Joint Range and Angle Estimation Using MIMO Radar With Frequency Diverse Array

Jingwei Xu, Guisheng Liao, *Member, IEEE*, Shengqi Zhu, *Member, IEEE*, Lei Huang, *Senior Member, IEEE*, and Hing Cheung So, *Fellow, IEEE*

***Abstract*—Phased array is widely used in radar systems with its beam steering fixed in one direction for all ranges. Therefore, the range of a target cannot be determined within a single pulse when range ambiguity exists. In this paper, an unambiguous approach for joint range and angle estimation is devised for multiple-input multiple-output (MIMO) radar with frequency diverse array (FDA). Unlike the traditional phased array, FDA is capable of employing a small frequency increment across the array elements. Because of the frequency increment, the transmit steering vector of the FDA-MIMO radar is a function of both range and angle. As a result, the FDA-MIMO radar is able to utilize degrees-of-freedom in the range-angle domains to jointly determine the range and angle parameters of the target. In addition, the Cramér–Rao bounds for range and angle are derived, and the coupling between these two parameters is analyzed. Numerical results are presented to validate the effectiveness of the proposed approach.**

***Index Terms*—Multiple-input multiple-output radar, frequency diverse array, range ambiguity, joint range and angle estimation, Cramér-Rao bound.**

I. Introduction

As multiple-input multiple-output (MIMO) radar [1]–[3] is a flexible technique which enjoys many advantages without sacrificing the excellence of the phased-array radar, it has recently received much attention. Unlike the traditional phased-array radar, the MIMO radar is able to efficiently employ the degrees-of-freedom (DOFs) in the temporal domain by emitting orthogonal waveforms and spatial domain by utilizing the array structure in transmit and receive antennas. This eventually leads to considerable enhancement in identifiability and resolution. Basically, there are two types of MIMO radar, that is, colocated MIMO radar [1] and distributed MIMO radar [2]. This work addresses the colocated MIMO radar.

Manuscript received September 26, 2014; revised January 17, 2015 and March 25, 2015; accepted April 01, 2015. Date of publication April 13, 2015; date of current version May 29, 2015. The associate editor coordinating the review of this manuscript and approving it for publication was Dr. Petr Tichavsky. This work was supported by the National Nature Science Foundation of China (NSFC) (Grants 61231017 and 91438106).

J. Xu, G. Liao, and S. Zhu are with the National Laboratory of Radar Signal Processing, Xidian University, Xi'an, Shaanxi, 710071, China (e-mail: xujingwei1987@163.com; zhushengqi8@163.com; gsliao@xidian.edu.cn).

L. Huang is with the College of Information Engineering, Shenzhen University, Shenzhen, 518052, China (e-mail: dr.lei.huang@ieee.org).

H. C. So is with the Department of Electronic Engineering, City University of Hong Kong, Hong Kong 852, China (e-mail: hcso@ee.cityu.edu.hk).

This paper has supplementary downloadable multimedia material available at http://ieeexplore.ieee.org provided by the authors. This file contains the MATLAB codes for reproducing the results in this work, which is made available for personal purpose. This material is 16 KB in size.

Color versions of one or more of the figures in this paper are available online at http://ieeexplore.ieee.org.

Digital Object Identifier 10.1109/TSP.2015.2422680

One of the foremost tasks of radar system is target localization for military or civilian purposes [4]. Each target is characterized by its range, angle, velocity and reflected complex amplitude. The phased-array radar can provide high-resolution angle estimation and thereby is widely used for target localization. It is known that by increasing the pulse repetition frequency (PRF) of radar, higher levels of clutter cancellation can be achieved and Doppler ambiguities can be eliminated. However, an increase in PRF may result in the maximum unambiguous range much smaller than the desired operating range [5]. The limitation of phased array is that its beam steering is fixed in only one direction for all ranges. Thus, the ranges of targets cannot be directly estimated from its beamforming output for high PRF radar in the presence of the inherent range ambiguity. A multiple PRF radar is utilized in [5], [6] to resolve the range ambiguity problem. In the multiple-target case, however, the ghost targets will appear when the range partnership errors exist. The staggered PRF and pulse-diverse waveform strategies could also mitigate the range ambiguity. Nevertheless, these techniques would incur difficulty in coherent processing in Doppler domain and lead to performance degradation in the extended clutter suppression [7], [8]. Although the distributed MIMO radar has been suggested in [9], [10] for unambiguous localization, the time and phase synchronization poses a big challenge for the MIMO radar with widely separated antennas. In this paper, we consider the colocated MIMO radar transmitting only one PRF to solve the range ambiguity problem even in the presence of multiple targets.

A flexible beam scanning array, referred to as frequency diverse array (FDA), was first introduced in [11]. The most important difference of the FDA from its traditional phased array counterpart is that the carrier frequency of the waveform is increased with a small amount across the array elements. As coherent waveform is radiated from each element of FDA, a range-angle-time-dependent beampattern is acquired [12]. The continuous beam scanning feature is evaluated by simulation examples in [13] and examined from a design perspective in [14]–[16]. The range-angle-dependent beampattern is utilized to suppress range-ambiguous clutter and improve moving target detection performance in [17]. It is shown in [18], [19] that, by exploiting the DOFs in the space, time, frequency and modulation domains, the radar waveforms can be constructed which serve multiple missions at the same time. An adaptive receive approach, namely, space-range adaptive processing, is proposed in [20] to mitigate space-range sidelobe. Sammartino *et al.* have proposed a frequency diverse bistatic system to generate a range-dependent beampattern in [21], [22], and merge the MIMO technique with FDA in [23], [24] where the fre-

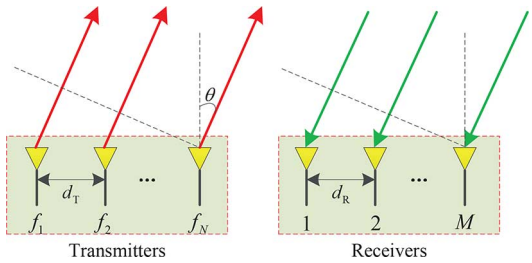

Fig. 1. Transmitters and receivers of a colocated MIMO radar.

quency offset is much smaller than the modulation bandwidth. Note that large frequency increment can decorrelate the coherence among the reflection coefficient of target, thus reducing the target fluctuation by exploiting radar cross section (RCS) diversity [25], [26]. A combination of phased-MIMO radar and FDA is explored in [27], [28]. The FDA is divided into subarrays and each subarray transmits coherent waveform. As a result, the range-angle-dependent beampattern is maintained. In [29], a joint range and angle estimation method is proposed for the FDA-MIMO radar by using the transmit sub-aperture optimization. The range and angle coupling is alleviated by forming the range and angle decoupled beampattern. In [30], two pulses with zero and non-zero frequency increments are transmitted with FDA radar, and a range and angle localization approach is proposed. This method firstly estimates the target angles with traditional phased array and then localizes the targets in range domain using FDA.

The Cramér-Rao bound (CRB) is usually used as a benchmark to assess unbiased estimators. The deterministic CRB is important for target parameter estimation since for a sufficiently high signal-to-noise ratio (SNR) and infinite number of observations, the performance of the deterministic maximum likelihood estimator (MLE) attains this bound [31]. In [32]–[35], the CRB of the direction parameter is derived for the colocated MIMO radar. The main focus of these techniques is to estimate the directions-of-arrival of targets located within a certain range-Doppler cell. The problem of estimating the location and velocity of a moving target is addressed in [36]–[38]. In [38], the CRBs of range, angle and velocity are derived for FDA radar, in which the transmit steering vector is considered and the FDA is divided into two subarrays to alleviate the coupling of range and angle. However, in some practical applications, the high PRF will cause the range ambiguity problem, thus calling for range estimation of the targets.

In this paper, the range-angle-dependent characteristic of FDA-MIMO radar is properly utilized and an unambiguous range and angle estimation method is proposed. Since the transmit steering vector depends on the range and angle parameters, the FDA-MIMO radar could introduce controllable transmit DOFs in the joint range-angle dimension. In the sequel, with the combination of the transmit and receive DOFs, the FDA-MIMO radar could obtain the range and angle estimation at the same time. Besides, a range ambiguity resolving technique is derived through a well-founded design of frequency increment. Additionally, closed-form expressions for the range and angle of the FDA-MIMO radar are devised. Note that the CRB computation assumes the presence of structured interference and background noise. Moreover, the coupling relationship of range and angle is analyzed.

The remainder of this paper is organized as follows. Section II formulates the signal model of the FDA-MIMO radar. In Section III, we present the joint range and angle estimation approach with range ambiguity resolved. The performance bound is derived in Section IV. Extensive simulation results are presented in Section V. Finally, conclusions are drawn in Section VI.

II. Signal Model of Colocated FDA-MIMO Radar

Consider a colocated MIMO radar system consisting of N transmit antennas and M receive antennas. The carrier frequency at the nth antenna is

$$f_n = f_0 + (n-1)\Delta f, \quad n = 1, 2, \ldots, N \tag{1}$$

where Δf is the frequency increment across the array elements and f_0 is the reference carrier frequency. The frequency increment is negligible compared with the carrier frequency and bandwidth of the transmitted waveform. Fig. 1 shows the configuration of the FDA-MIMO radar.

The transmitted signal of the nth element can be expressed as

$$s_n(t) = \sqrt{\frac{E}{N}}\phi_n(t)e^{j2\pi f_n t}, \quad 0 \le t \le T, \quad n = 1, 2, \ldots, N \tag{2}$$

where E is the total transmitted energy, T is the radar pulse duration and $\phi_n(t)$ denotes the unity-energy waveform, i.e., $\int_0^T \phi_n(t)\phi_n^*(t)dt = 1, n = 1, 2, \ldots, N$ where the superscript * stands for the conjugate operator. We assume that the waveforms satisfy the orthogonality condition

$$\int_T \phi_m(t)\phi_n^*(t-\tau)e^{j2\pi\Delta f(m-n)t}dt = 0, \ m \ne n, \forall\tau \tag{3}$$

where τ is the time shift.

It is assumed that the electromagnetic wave is independently propagating in the free space. Herein, we consider the two-way propagation case and choose the first element as the reference point. Thus, for an arbitrary target, the received echo of the mth element can be written as

$$y_m(t) = \sum_{n=1}^{N}\left\{\sqrt{\frac{E}{N}}\xi\phi_n(t-\tau_{n,\mathrm{T}}-\tau_{m,\mathrm{R}}) \times e^{j2\pi(f_n+f_{d,n})(t-\tau_{n,\mathrm{T}}-\tau_{m,\mathrm{R}})}\right\} \tag{4}$$

where ξ is the complex-valued reflection coefficient of the target, $f_{d,n}$ denotes the Doppler frequency, i.e., $f_{d,n} = 2v_t/\lambda_n$, v_t is the radial velocity of the target, $\lambda_n = c/f_n$ is the wavelength corresponding to the nth transmit antenna and $\lambda_0 = c/f_0$ is the reference wavelength. Actually, the Doppler frequency can be approximately expressed as $f_d = 2v_t/\lambda_0$ since the frequency increment is negligible compared with the carrier frequency. Moreover, $\tau_{n,\mathrm{T}}$ and $\tau_{m,\mathrm{R}}$ are the transmit and receive time delays, respectively, which are given as

$$\begin{aligned}\tau_{n,\mathrm{T}} &= \frac{1}{c}[r - d_{\mathrm{T}}(n-1)\sin(\theta)] = \frac{\tau_0}{2} - \frac{d_{\mathrm{T}}}{c}(n-1)\sin(\theta)\\ \tau_{m,\mathrm{R}} &= \frac{1}{c}[r - d_{\mathrm{R}}(m-1)\sin(\theta)] = \frac{\tau_0}{2} - \frac{d_{\mathrm{R}}}{c}(m-1)\sin(\theta)\end{aligned} \tag{5}$$

where $\tau_0 = 2r/c$, θ stands for the angle of the target (measured from the normal direction to the target direction) and r is the range of the target while d_{T} and d_{R} are the interspacings of transmit and receive antennas, respectively.

In the receive array, the measured signals are down converted, matched filtered and stored. The received signal can be decomposed by N matched filters, yielding N isolated transmitted signals. The matched filter is expressed as $\phi_n(t)e^{j2\pi(n-1)\Delta ft}, n = 1, 2, \ldots, N$. After matched filtering, the nth output of the mth received antenna is

$$\begin{aligned} y_{mn} &\approx \sqrt{\frac{E}{N}}\xi e^{j2\pi f_d(t-\tau_0)}e^{-j2\pi\frac{f_n}{c}2r} \\ &\quad \times e^{j2\pi\frac{f_n}{c}[d_{\mathrm{T}}(n-1)\sin(\theta)+d_{\mathrm{R}}(m-1)\sin(\theta)]} \\ &\approx \sqrt{\frac{E}{N}}\xi e^{j2\pi f_d(t-\tau_0)}e^{-j4\pi\frac{f_0}{c}r} \\ &\quad \times e^{-j4\pi\frac{\Delta f}{c}(n-1)r}e^{j2\pi\frac{f_0}{c}[d_{\mathrm{T}}(n-1)\sin(\theta)+d_{\mathrm{R}}(m-1)\sin(\theta)]} \end{aligned} \tag{6}$$

Similarly, the approximation in (6) is obtained based on the fact that the frequency increment is relatively negligible [24]. Thus the output of the mth element can be written as a vector

$$\mathbf{y}_m = \sqrt{\frac{E}{N}}\xi \begin{bmatrix} 1 \\ e^{-j4\pi\frac{\Delta f}{c}r+j2\pi\frac{d_{\mathrm{T}}}{\lambda_0}\sin(\theta)} \\ \vdots \\ e^{-j4\pi\frac{\Delta f}{c}(N-1)r+j2\pi\frac{d_{\mathrm{T}}}{\lambda_0}(N-1)\sin(\theta)} \end{bmatrix} \times e^{j2\pi\frac{d_{\mathrm{R}}}{\lambda_0}(m-1)\sin(\theta)} \tag{7}$$

where $\mathbf{y}_m \in \mathbb{C}^{N\times 1}$. The term $e^{j2\pi f_d(t-\tau_0)}e^{-j4\pi f_0 r/c}$ in (6) is absorbed into the reflection coefficient ξ and herein we do not include it for the sake of simplicity. Thus the virtual data snapshot of the target signal can be expressed as

$$\mathbf{x_s} = \left[\mathbf{y}_1^{\mathrm{T}}, \mathbf{y}_2^{\mathrm{T}}, \ldots, \mathbf{y}_M^{\mathrm{T}}\right]^{\mathrm{T}} = \sqrt{\frac{E}{N}}\xi\mathbf{b}(\theta)\otimes\mathbf{a}(r,\theta) \tag{8}$$

where the superscript $^{\mathrm{T}}$ denotes the transpose operator, $\otimes$ is the Kronecker product [39], $\mathbf{a}(r,\theta) \in \mathbb{C}^{N\times 1}$ and $\mathbf{b}(\theta) \in \mathbb{C}^{M\times 1}$ are the transmit and receive steering vectors, respectively, defined as

$$\mathbf{a}(r,\theta) = \begin{bmatrix} 1 \\ e^{-j4\pi\frac{\Delta f}{c}r+j2\pi\frac{d_{\mathrm{T}}}{\lambda_0}\sin(\theta)} \\ \vdots \\ e^{-j4\pi\frac{\Delta f}{c}(N-1)r+j2\pi\frac{d_{\mathrm{T}}}{\lambda_0}(N-1)\sin(\theta)} \end{bmatrix} \tag{9}$$

$$\mathbf{b}(\theta) = \left[1, e^{j2\pi\frac{d_{\mathrm{R}}}{\lambda_0}\sin(\theta)}, \ldots, e^{j2\pi\frac{d_{\mathrm{R}}}{\lambda_0}(M-1)\sin(\theta)}\right]^{\mathrm{T}}. \tag{10}$$

It follows from (9) and (10) that this model can be simplified to the traditional fixed carrier frequency MIMO radar if the frequency increment is zero. As shown in (9), the transmit steering vector is not only angle-dependent but also range-dependent, i.e.,

$$\mathbf{a}(r,\theta) = \mathbf{r}(r)\odot\mathbf{d}(\theta) \tag{11}$$

where $\odot$ is the Hadamard (element-wise) product, $\mathbf{r}(r) = [1, e^{-j4\pi\Delta fr/c}, \ldots, e^{-j4\pi\Delta f(N-1)r/c}]^{\mathrm{T}}$ is the transmit range steering vector and $\mathbf{d}(\theta) = [1, e^{j2\pi d_{\mathrm{T}}\sin(\theta)/\lambda_0}, \ldots, e^{j2\pi d_{\mathrm{T}}(N-1)\sin(\theta)/\lambda_0}]^{\mathrm{T}}$ is the transmit angular steering vector. Therefore, the FDA-MIMO radar could utilize the transmit and receive DOFs to determine the range and angle of the target.

Assume that there are L jamming signals impinging on the array from directions $\theta_l, l = 1, 2, \ldots, L$. The received interference can be expressed as

$$\mathbf{x_i} = \sum_{l=1}^{L}\xi_l\mathbf{b}(\theta_l)\otimes\mathbf{n_a}_l \tag{12}$$

where ξ_l is zero-mean circularly symmetric complex Gaussian random variable with variance $\sigma_l^2 = \mathbb{E}\{\xi_l\xi_l^*\}, l = 1, 2, \ldots, L$. Here $\mathbb{E}\{\cdot\}$ is the mathematical expectation. The $\mathbf{n_a}_l \in \mathbb{C}^{N\times 1}$ and $\mathbf{b}(\theta_l) \in \mathbb{C}^{M\times 1}$ are, respectively, the corresponding noise-like transmit steering vector and receive steering vector of the noise jamming [40]. The interferences are statistically noise-like and oppressive. Thus, $\mathbf{n_a}_l$ is also assumed zero-mean white Gaussian distributed, i.e., $\mathbf{n_a}_l \sim \mathcal{CN}(\mathbf{0}, \mathbf{I}_N)$, where $\mathbf{0}$ is $N \times 1$ zero vector and $\mathbf{I}_N$ is the $N \times N$ identity matrix. The receive steering vector takes the form of $\mathbf{b}(\theta_l) = [1, e^{j2\pi d\sin(\theta_l)/\lambda_0}, \ldots, e^{j2\pi d(M-1)\sin(\theta_l)/\lambda_0}]^{\mathrm{T}}$. Since the interferences are independent of each other, the covariance matrix can be calculated as

$$\begin{aligned} \mathbf{R} &= \mathbb{E}\left\{\mathbf{x}_i\mathbf{x}_i^{\mathrm{H}}\right\} \\ &= \mathbb{E}\left\{\sum_{l=1}^{L}\xi_l\xi_l^*[\mathbf{b}(\theta_l)\otimes\mathbf{n_a}_l][\mathbf{b}(\theta_l)\otimes\mathbf{n_a}_l]^{\mathrm{H}}\right\} \\ &= \sum_{l=1}^{L}\sigma_l^2\mathbf{b}(\theta_l)\mathbf{b}^{\mathrm{H}}(\theta_l)\otimes\mathbf{I}_N \end{aligned} \tag{13}$$

where the superscript $^{\mathrm{H}}$ is the conjugate transpose operator. The total received data snapshot is written as

$$\begin{aligned} \mathbf{x} &= \mathbf{x}_s + \mathbf{x}_i + \mathbf{x}_n \\ &= \sqrt{\frac{E}{N}}\xi\mathbf{b}(\theta)\otimes\mathbf{a}(r,\theta) + \sum_{l=1}^{L}\xi_l\mathbf{b}(\theta_l)\otimes\mathbf{n_a}_l + \mathbf{x}_n \end{aligned} \tag{14}$$

where $\mathbf{x}_n$ is the independent noise which is assumed to be a zero-mean white circularly Gaussian vector with covariance $\sigma^2\mathbf{I}_{MN}$. Herein, the target of interest is assumed to be an unknown deterministic signal. In this case, the observation vector $\mathbf{x}$ follows a Gaussian distribution with mean $\mathbf{x}_s$ and covariance matrix $\mathbf{Q} = \mathbf{R} + \sigma^2\mathbf{I}_{MN}$.

III. Unambiguous Range-Angle Estimation

In this section, we propose an unambiguous approach for joint range and angle estimation by exploiting the property of the FDA-MIMO radar, that is, it is able to provide resolvability in range and angle. Note that this resolvability depends on the frequency increment. Thus, we derive the metrics to determine the frequency increment.

A. Range Dependence Compensation

Compared with the traditional MIMO radar, the transmit steering vector of FDA-MIMO radar is both range and angle dependent. Based on the analysis in Section II, we define the transmit spatial frequency $f_{s,\mathrm{T}}$ and receive spatial frequency $f_{s,\mathrm{R}}$ as

$$f_{s,\mathrm{T}} = f_r + f_{a,\mathrm{T}} = -\frac{2\Delta f}{c}r + \frac{d_{\mathrm{T}}}{\lambda_0}\sin(\theta) \tag{15a}$$

$$f_{s,\mathrm{R}} = \frac{d_{\mathrm{R}}}{\lambda_0}\sin(\theta) \tag{15b}$$

where $f_r = -2\Delta f r/c$ and $f_{a,\mathrm{T}} = d_{\mathrm{T}} \sin(\theta)/\lambda_0$ are defined as the range frequency and angular frequency, respectively. Since the transmit spatial frequency of the FDA-MIMO radar is dependent on range and angle, the distribution of target in the joint transmit-receive spatial frequency domains of the FDA-MIMO radar is different from that of the traditional MIMO radar. In the latter, the transmit spatial frequency is always a linear function of the receive spatial frequency, i.e., $f_{s,\mathrm{T}}/f_{s,\mathrm{R}} = d_{\mathrm{T}}/d_{\mathrm{R}}$. In particular, when the interspacings of the transmit and receive antennas are identical, the spectrum of target is diagonally distributed in the joint transmit-receive spatial frequency domains. In contrast, this diagonal structure is destroyed in the FDA-MIMO radar. Indeed, it follows from (15) that the transmit spatial frequency is composed of the range and angular frequencies. Thus, the target can be arbitrarily distributed in the joint transmit-receive spatial frequency domains.

Assume that an estimate of the range frequency is obtained, which satisfies the condition of $\max\{|f_r|\} < 1$. In this scenario, the range can be estimated without ambiguity. Besides, the mean and variance of the range estimate can be expressed, respectively, as

$$\mathbb{E}\{r\} = -\frac{c}{2\Delta f}\mathbb{E}\{f_r\}$$
$$\mathrm{cov}\{r\} = \left(\frac{c}{2\Delta f}\right)^2 \mathrm{cov}\{f_r\}$$

where $\mathrm{cov}\{\cdot\}$ is the covariance operator. Therefore, the smaller $c/(2\Delta f)$ is (or the larger the frequency increment is), the more accurate the range estimation will be. However, in order to guarantee that $\max\{|f_r|\} < 1$, the frequency increment Δf should satisfy

$$\frac{c}{2\Delta f} > r_{\max} \tag{16}$$

where $r_{\max}$ is the maximum detectable range of the radar. It should be noted that, although the range ambiguity can be resolved, the range estimation accuracy is not higher than that of the traditional range estimation in this case. In what follows, we propose an approach to resolve the range ambiguity and yield accurate range estimation.

As stated in (15), the transmit spatial frequency is range-dependent. This range dependence can be compensated by applying a compensating vector range-by-range on the received data. The compensating vector in the transmit spatial frequency domain can be expressed as

$$\mathbf{h}(r_b) = \left[1, e^{j2\pi\frac{2\Delta f}{c}r_b}, \ldots, e^{j2\pi\frac{2\Delta f}{c}(N-1)r_b}\right]^{\mathrm{T}} \tag{17}$$

where r_b is the *a priori* range estimate, which is calculated with the range bin number and bin size. In the traditional radar, the accuracy of the range estimate is determined by the bandwidth of the transmitted signal, which cannot be further improved. In contrast, the range estimation accuracy is improved in FDA-MIMO radar because of the range dependence of the steering vector.

In the presence of range ambiguity, the true range of the target is written as

$$r = r_a + (p-1)r_u \tag{18}$$

where r_a is the principal range of the target, p is the index of range ambiguity of the target and $p \in [1, N_a]$, where N_a denotes the number of ambiguous ranges and $r_u = c/(2f_{\mathrm{PRF}})$ is the maximum unambiguous range with f_{PRF} denoting the PRF. Note that the *a priori* range estimate r_b approximately equals the principal range r_a. We define the principal range difference as

$$r_\Delta = r_a - r_b \tag{19}$$

which is a random variable uniformly distributed between $[-\frac{c}{4B}, \frac{c}{4B}]$, where B is the bandwidth of the transmitted signal. In traditional MIMO radar, this principal range difference cannot be estimated. In contrast, for the FDA-MIMO radar, it can be determined since the transmit spatial frequency of the FDA-MIMO radar is dependent on the range.

As shown in (15), the receive spatial frequency of the FDA-MIMO radar is independent of the range. Thus, the compensating vector in the joint transmit-receive spatial frequency domains can be expressed as

$$\mathbf{g} = \mathbf{1}_M \otimes \mathbf{h}(r_b) \tag{20}$$

where $\mathbf{1}_M$ is $M \times 1$ vector with all elements are equal to one. After compensation, the received data can be expressed as

$$\begin{aligned}
\mathbf{x}_{\mathrm{comp}} = \mathbf{x} \odot \mathbf{g} &= \left(\sqrt{\frac{E}{N}}\xi\mathbf{b}(\theta) \otimes \mathbf{a}(r,\theta) \right.\\
&\quad \left. + \sum_{l=1}^{L} \xi_l \mathbf{b}(\theta_l) \otimes \mathbf{n}_{\mathbf{a}l} + \mathbf{x}_n\right) \odot \mathbf{g}\\
&= \sqrt{\frac{E}{N}}\xi\mathbf{b}(\theta) \otimes [\mathbf{r}(r) \odot \mathbf{d}(\theta) \odot \mathbf{h}(r_b)]\\
&\quad + \sum_{l=1}^{L} \xi_l \mathbf{b}(\theta_l) \otimes [\mathbf{n}_{\mathbf{a}l} \odot \mathbf{h}(r_b)] + \mathbf{x}_n \odot \mathbf{g}\\
&= \sqrt{\frac{E}{N}}\xi\mathbf{b}(\theta) \otimes [\mathbf{r}(r - r_b) \odot \mathbf{d}(\theta)]\\
&\quad + \sum_{l=1}^{L} \xi_l \mathbf{b}(\theta_l) \otimes [\mathbf{n}_{\mathbf{a}l} \odot \mathbf{h}(r_b)] + \mathbf{x}_n \odot \mathbf{g}\\
&= \sqrt{\frac{E}{N}}\xi\mathbf{b}(\theta) \otimes [\mathbf{r}\left(r_\Delta + (p-1)r_u\right) \odot \mathbf{d}(\theta)]\\
&\quad + \sum_{l=1}^{L} \xi_l \mathbf{b}(\theta_l) \otimes [\mathbf{n}_{\mathbf{a}l} \odot \mathbf{h}(r_b)] + \mathbf{x}_n \odot \mathbf{g}
\end{aligned} \tag{21}$$

As aforementioned, the received noise is zero-mean white circularly Gaussian distributed in the joint transmit-receive domains while the interferences are zero-mean white circularly Gaussian distributed only in transmit dimension. Since the compensation procedure in (21) is also conducted in transmit dimension, it has no influence on the spectrum distribution of the interference and noise. Thus, the signal model in (21) can be equivalently rewritten as

$$\mathbf{x}_{\mathrm{comp}} = \sqrt{\frac{E}{N}}\xi\mathbf{b}(\theta) \otimes [\mathbf{r}(r_\Delta + (p-1)r_u) \odot \mathbf{d}(\theta)] + \mathbf{x}_i + \mathbf{x}_n \tag{22}$$

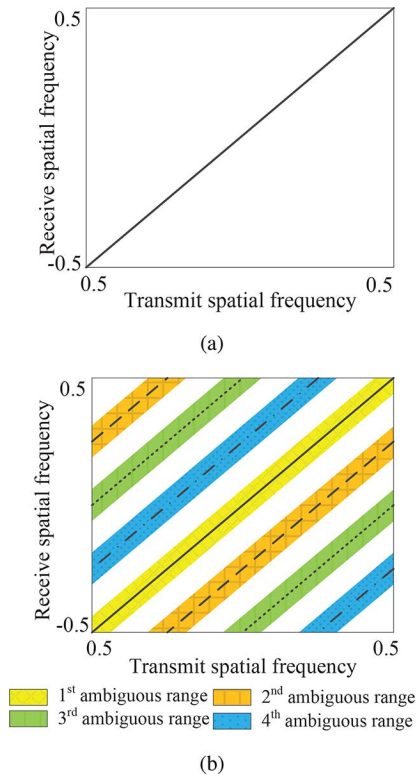

Fig. 2. Spectrum distribution of the target in the presence of range ambiguity. (a) Traditional MIMO radar and (b) FDA-MIMO radar.

After compensation, the transmit spatial frequency is expressed as

$$f_{s-\mathrm{comp,T}} = f_{r-\mathrm{comp}} + f_{a,\mathrm{T}} = -\frac{2\Delta f}{c}[r_\Delta + (p-1)r_u] + \frac{d_\mathrm{T}}{\lambda_0}\sin(\theta) \quad (23)$$

where $f_{s-\mathrm{comp}}$ is the compensated range frequency, i.e.,

$$f_{r-\mathrm{comp}} = -\frac{2\Delta f}{c}[r_\Delta + (p-1)r_u] \quad (24)$$

Since the principal range difference r_Δ is relatively small, the compensated transmit spatial frequency of the target in the FDA-MIMO radar can be viewed as a shift of the transmit spatial frequency in the traditional MIMO radar by a factor corresponding to the index of range ambiguity p.

Fig. 2 shows the comparison of the spectrum distribution of the target in the presence of range ambiguity in the traditional MIMO radar and FDA-MIMO radar. Herein, we consider the case of $d_\mathrm{T} = d_\mathrm{R}$ and $N_a = 4$. For the traditional colocated MIMO radar, the transmit and receive spatial frequencies depend on the angle only. Thus, the spectrum of the target in the joint transmit-receive spatial frequency domains is diagonally distributed and the range ambiguity cannot be resolved. In contrast, after compensated, the spectrum distribution of the target in the FDA-MIMO radar is distinguishable for different ambiguous ranges. The targets from different ambiguous ranges will appear in the corresponding straps. Note that the width of strap is caused by the uncertainty of the principal range difference.

By decomposing the ratio of the frequency increment to the PRF into two parts: the non-negative integer part and the decimal part, we have

$$\frac{\Delta f}{f_\mathrm{PRF}} = q + v \quad (25)$$

where $q \in \mathbb{N}$ and $v \in [0,1)$. Note that q and v are constant scalars which can be calculated once the radar parameters, namely, Δf and f_PRF, are given. Substituting (25) into (24) yields

$$f_{r-\mathrm{comp}} = -\frac{2\Delta f}{c}r_\Delta - (p-1)(q+v). \quad (26)$$

It can be concluded that range estimation is equivalent to determining r_Δ and p. Therefore, the range ambiguity is resolved and the accuracy of the range estimate can be improved.

B. Joint Range and Angle Estimation

Since the range and angle of the target are coupled in transmit dimension, they cannot be directly estimated from (22). Actually, as we have analyzed, the transmit spatial frequency is dependent on both range and angle while the receive spatial frequency only depends on the angle. Based on this fact, we propose an unambiguous range and angle estimation approach. In particular, we firstly estimate the angle of the target using the compensated data in receive dimension. Then, we determine the index of range ambiguity p. Finally, we estimate the principal range difference r_Δ. Thus, this unambiguous range and angle estimation approach can be interpreted as detecting the targets in receive spatial frequency domain and then resolving the range ambiguity and estimating the range in the joint transmit-receive spatial frequency domains. The joint range and angle estimation method is described as follows.

For the range cell under test, we reconstruct the compensated data snapshot into an $M \times N$ data matrix $\mathbf{X}_\mathrm{comp}$.

$$\mathbf{X}_\mathrm{comp} = [\mathrm{mat}(\mathbf{x}_\mathrm{comp})]^\mathrm{T} = \sqrt{\frac{E}{N}}\xi\mathbf{b}(\theta)\left[\mathbf{r}\left(r_\Delta + (p-1)r_u\right) \odot \mathbf{d}(\theta)\right]^\mathrm{T} + \mathbf{X}_i + \mathbf{X}_n \quad (27)$$

where $\mathrm{mat}(\cdot)$ denotes the reconstruction operator. The nth column of $\mathbf{X}_\mathrm{comp}$ is $\mathbf{X}_\mathrm{comp}(n) \in \mathbb{C}^{M\times 1}$, which contains the receive data corresponding to the nth transmit element.

The angle of the target is estimated by the MLE.

$$\hat{\theta} = \arg\max_\theta \left| \sum_{n=1}^{N} \mathbf{w}_\mathrm{R}^\mathrm{H}(\theta)\mathbf{X}_\mathrm{comp}(n) \right| \quad (28)$$

where $\mathbf{w}_\mathrm{R}(\theta) = \mathbf{Q}_\mathrm{R}^{-1}\mathbf{b}(\theta)$ is the minimum variance distortionless response (MVDR) adaptive weight with $\mathbf{Q}_\mathrm{R}$ is the interference-plus-noise covariance matrix in receive domain.

With the estimated angle, we construct the adaptive weight in the joint transmit-receive domains as

$$\mathbf{w}(p,0,\hat{\theta}) = \mathbf{Q}^{-1}\mathbf{u}(p,0,\hat{\theta}) \quad (29)$$

where $\mathbf{Q}$ is the corresponding interference-plus-noise covariance matrix in the joint transmit-receive dimensions,

$\mathbf{u}(p,0,\hat{\theta}) = \mathbf{b}(\hat{\theta}) \otimes [\mathbf{r}((p-1)r_u) \odot \mathbf{d}(\hat{\theta})]$ is the joint transmit-receive steering vector of the target.

The index of the range ambiguity is estimated as

$$\hat{p} = \arg \max_{p=1,2,\ldots,N_a} \left| \mathbf{w}^{\mathrm{H}}(p,0,\hat{\theta}) \mathbf{x}_{\mathrm{comp}} \right| \tag{30}$$

Using the estimated angle and index of the range ambiguity, the adaptive weight is

$$\mathbf{w}(\hat{p}, r_\Delta, \hat{\theta}) = \mathbf{Q}^{-1} \mathbf{u}(\hat{p}, r_\Delta, \hat{\theta}) \tag{31}$$

where $r_\Delta \in [-\frac{c}{4B}, \frac{c}{4B}]$. Thus, the principal range difference is estimated as

$$\hat{r}_\Delta = \arg \max_{r_\Delta} \left| \mathbf{w}^{\mathrm{H}}(\hat{p}, r_\Delta, \hat{\theta}) \mathbf{x}_{\mathrm{comp}} \right| \tag{32}$$

The range of the target is estimated as

$$\hat{r} = r_b + \hat{r}_\Delta + (\hat{p}-1) r_u. \tag{33}$$

After the angle, index of the range ambiguity and principal range difference are determined, the minimum mean-squared error (MMSE) beamformer is formulated as [41]

$$\begin{aligned} &\min_{\mathbf{w}_{\mathrm{MMSE}}} \max_{b_L \le |\xi| \le b_U} \mathbb{E}\{|\hat{\xi} - \xi|^2\} \\ &= \min_{\mathbf{w}_{\mathrm{MMSE}}} \max_{b_L \le |\xi| \le b_U} \left\{ \begin{array}{c} \mathbf{w}_{\mathrm{MMSE}}^{\mathrm{H}} \mathbf{Q} \mathbf{w}_{\mathrm{MMSE}} \\ -|\xi|^2 \left(1 - \mathbf{w}_{\mathrm{MMSE}}^{\mathrm{H}} \mathbf{u}\left(\hat{p}, \hat{r}_\Delta, \hat{\theta}\right)\right) \end{array} \right\} \end{aligned} \tag{34}$$

The adaptive weight is calculated as

$$\mathbf{w}_{\mathrm{MMSE}} = \mu_{\mathrm{MMSE}} \mathbf{Q}^{-1} \mathbf{u}(\hat{p}, \hat{r}_\Delta, \hat{\theta}) \tag{35}$$

where

$$\mu_{\mathrm{MMSE}} = \frac{b_U^2}{1 + b_U^2 \gamma} \tag{36}$$

and

$$\mu_{\mathrm{MMSE}} = \frac{1}{\gamma} \left(1 - \frac{1}{\sqrt{(1 + b_L^2 \gamma)(1 + b_U^2 \gamma)}} \right) \tag{37}$$

for min-max mean-squared error beamformer and min-max regret beamformer [41], respectively, where $\gamma = \mathbf{u}^{\mathrm{H}}(\hat{p}, \hat{r}_\Delta, \hat{\theta}) \mathbf{Q}^{-1} \mathbf{u}(\hat{p}, \hat{r}_\Delta, \hat{\theta})$. Thus, ξ is estimated as

$$\hat{\xi} = \mathbf{w}_{\mathrm{MMSE}}^{\mathrm{H}} \mathbf{x}_{\mathrm{comp}} = \mu_{\mathrm{MMSE}} \mathbf{u}^{\mathrm{H}}(\hat{p}, \hat{r}_\Delta, \hat{\theta}) \mathbf{Q}^{-1} \mathbf{x}_{\mathrm{comp}}. \tag{38}$$

The proposed unambiguous range and angle estimation algorithm is summarized in Table I.

C. Selection of Frequency Increment

In order to determine the index of range ambiguity accurately, the frequency increment should be correctly chosen. This subsection devises a scheme for optimizing the frequency increment Δf.

Because of the periodicity of the spatial frequency, the normalized compensated range frequency in (26) can be further expressed as

$$\tilde{f}_{r-\mathrm{comp}} = -\frac{2\Delta f}{c} r_\Delta - (p-1)v \tag{39}$$

Note that the integer $(p-1)q$ has been dropped in (39). Since the principal range difference is within $[-\frac{c}{4B}, \frac{c}{4B}]$, the index of range ambiguity can be accurately estimated if and only if the following conditions are satisfied

TABLE I
UNAMBIGUOUS RANGE AND ANGLE ESTIMATION METHOD

Step 1:	Construct the compensating vector with the *a priori* range estimate of the target using (20).
Step 2:	Perform compensation procedure to acquire the compensated data using (22).
Step 3:	Rearrange the received data snapshot into a matrix and estimate the angle of the target using (28).
Step 4:	Estimate the index of range ambiguity and the principal range difference of the target using (30) and (32), respectively. Finally, the range estimate is given by (33).
Step 5:	Estimate the coefficient of target based on MMSE criterion using (38).

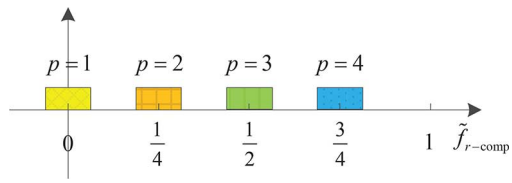

Fig. 3. Normalized range frequency distribution region with respect to index of range ambiguity.

$$v > 0 \tag{40a}$$

$$\max |\tilde{f}_{r-\mathrm{comp}}| < 1 \tag{40b}$$

$$\max \left| \frac{2\Delta f}{c} r_\Delta \right| < \frac{v}{2} \tag{40c}$$

Herein, (40a) guarantees the discriminability of different p for targets. Besides, (40b) should be satisfied in order to avoid periodic ambiguity. Moreover, it is desired that the maximum value of $\tilde{f}_{r-\mathrm{comp}}$ approaches 1 so that the targets from different ambiguous ranges can be distinguished easily. The third constraint (40c) guarantees that there is no influence on the estimation of p when the principal range difference varies within $[-\frac{c}{4B}, \frac{c}{4B}]$. Here, we give a more strict form of the constraints as

$$0 < N_a v \le 1 \tag{41a}$$

$$\max \left| \frac{2\Delta f}{c} r_\Delta \right| < \frac{v}{4} \tag{41b}$$

Fig. 3 provides an example for a given estimated angle at $N_a = 4$ and $v = 1/4$. The shadow regions indicate the possible values of range frequencies of the targets with the corresponding index of range ambiguity p. As p is an integer, it can be determined accurately if there is no overlap between adjacent ambiguous ranges. After p is determined, the principal range difference can be estimated. Therefore, not only the range ambiguity is resolved but also the range estimation accuracy is improved.

Under the constraints in (41), we can determine the optimal choice of the frequency increment as

$$\Delta f = \max_q \{(q+v) f_{\mathrm{PRF}}\}, \quad q \in \mathbb{N}$$
$$\text{s.t.} \begin{cases} v = \dfrac{1}{N_a} \\ \Delta f \le \dfrac{vB}{2} = \dfrac{B}{2N_a} \end{cases} \tag{42}$$

It follows from (42) that the frequency increment can be optimally chosen from a series of discrete values. As aforementioned, a larger frequency increment could improve the range estimation accuracy.

Note that large frequency increment can decorrelate the coherence among the reflection coefficients of target [25], [26]. In order to guarantee the coherence of the reflection coefficients, (42) can be further modified as

$$\Delta f = \max_{q}\{(q+v)f_{\mathrm{PRF}}\}, \quad q \in \mathbb{N} \quad \text{s.t.} \begin{cases} v = \dfrac{1}{N_a} \\ \Delta f \le \min\left\{\dfrac{B}{2N_a}, \dfrac{B}{N-1}\alpha\right\} \end{cases} \tag{43}$$

where $\alpha = \frac{(N-1)\Delta f}{B} \in (0,1)$.

Since the range parameter estimation is transformed into the estimation of the range frequency of the target, the identifiability of the number of ambiguous ranges is determined by $\max\{N_a\} = \mathrm{int}(\frac{N-1}{2})$ [42]. Herein $\mathrm{int}(x)$ indicates the smallest integer greater than or equal to x. Hence, the maximum number of targets which can be uniquely identified by a FDA-MIMO radar is proportional to the number of transmit antennas.

IV. Performance Analysis

In this section, we study the performance lower bound of the FDA-MIMO radar by deriving the CRBs for the range and angle. Moreover, the coupling between range and angle parameters is analyzed.

The unknown parameter vector is

$$\begin{aligned}\Psi &= \left[\boldsymbol{\alpha}^{\mathrm{T}}, \boldsymbol{\beta}^{\mathrm{T}}\right]^{\mathrm{T}} \\ &= \left[r, \theta, \bar{\xi}, \breve{\xi}, \theta_1, \ldots, \theta_L, \bar{\xi}_1, \ldots, \bar{\xi}_L, \breve{\xi}_1, \ldots, \breve{\xi}_L, \sigma\right]^{\mathrm{T}}\end{aligned} \tag{44}$$

where the deterministic parameters of the target signal are collected in $\boldsymbol{\alpha} = [r, \theta, \bar{\xi}, \breve{\xi}]^{\mathrm{T}}$ with $\bar{\xi} = \mathrm{Re}\{\xi\}$ and $\breve{\xi} = \mathrm{Im}\{\xi\}$, respectively. The parameters of the interferences and noise are collected in $\boldsymbol{\beta} = [\theta_1, \ldots, \theta_L, \bar{\xi}_1, \ldots, \bar{\xi}_L, \breve{\xi}_1, \ldots, \breve{\xi}_L, \sigma]^{\mathrm{T}}$. Since the parameters of interest and nuisance are decoupled, the Fisher information matrix (FIM) for Ψ is block-diagonal. Thus, the CRBs for the parameters of interest can be independently derived as

$$\mathbf{D}_{\boldsymbol{\alpha}}^{-1} = \mathbf{F} = \frac{2KE}{N}\mathrm{Re}\left\{\left(\frac{\partial \xi \mathbf{u}(r,\theta)}{\partial \boldsymbol{\alpha}}\right)^{\mathrm{H}} \mathbf{Q}^{-1}\left(\frac{\partial \xi \mathbf{u}(r,\theta)}{\partial \boldsymbol{\alpha}}\right)\right\} \tag{45}$$

where $\mathbf{u}(r,\theta) = \mathbf{b}(\theta) \otimes [\mathbf{r}(r-r_b) \odot \mathbf{d}(\theta)]$ is the joint transmit-receive steering vector of the target after compensation and K is the number of snapshots. Define three auxiliary vectors as $\mathbf{w} = \mathbf{Q}^{-1/2}\mathbf{u}(r,\theta)$, $\mathbf{w}_r = \mathbf{Q}^{-1/2}\mathbf{u}_r(r,\theta)$, $\mathbf{w}_\theta = \mathbf{Q}^{-1/2}\mathbf{u}_\theta(r,\theta)$, where $\mathbf{Q}^{-1/2}$ is the square root matrix of the positive definite matrix $\mathbf{Q}^{-1}$ such that $\mathbf{Q}^{-1/2}\mathbf{Q}^{-1/2} = \mathbf{Q}^{-1}$ and

$$\mathbf{u}_r(r,\theta) = \frac{\partial \mathbf{u}(\theta, r)}{\partial r} = \mathbf{b}(\theta) \otimes \left[\frac{\partial \mathbf{r}(r-r_b)}{\partial r} \odot \mathbf{d}(\theta)\right] \tag{46a}$$

$$\begin{aligned}\mathbf{u}_\theta(r,\theta) = \frac{\partial \mathbf{u}(\theta, r)}{\partial \theta} &= \frac{\partial \mathbf{b}(\theta)}{\partial \theta} \otimes [\mathbf{r}(r-r_b) \odot \mathbf{d}(\theta)] \\ &\quad + \mathbf{b}(\theta) \otimes \left[\mathbf{r}(r-r_b) \odot \frac{\partial \mathbf{d}(\theta)}{\partial \theta}\right]\end{aligned} \tag{46b}$$

where

$$\frac{\partial \mathbf{r}(r-r_b)}{\partial r} = j2\pi\frac{2\Delta f}{c}\mathbf{E}_{\mathbf{r}}\mathbf{r}(r-r_b),$$

$$\frac{\partial \mathbf{b}(\theta)}{\partial \theta} = j2\pi\frac{f_0}{c}d_{\mathrm{R}}\cos(\theta)\mathbf{E}_{\mathbf{b}}\mathbf{b}(\theta)$$

and

$$\frac{\partial \mathbf{d}(\theta)}{\partial \theta} = j2\pi\frac{f_0}{c}d_{\mathrm{T}}\cos(\theta)\mathbf{E}_{\mathbf{d}}\mathbf{d}(\theta).$$

Here, $\mathbf{E}_{\mathbf{r}} = \mathbf{E}_{\mathbf{d}} = \mathrm{diag}(0, 1, \ldots, N-1)$ and $\mathbf{E}_{\mathbf{b}} = \mathrm{diag}(0, 1, \ldots, M-1)$. The FIM can be expressed as (47) at the bottom of the page.

Utilizing the Schur complement, the inverse of the FIM can be expressed as

$$\mathbf{D}_\alpha = \mathbf{F}^{-1} = \frac{N}{2KE}\begin{bmatrix}\mathbf{F}_{11} & \mathbf{F}_{12} \\ \mathbf{F}_{21} & \mathbf{F}_{22}\end{bmatrix}^{-1} = \frac{N}{2KE}\left[\begin{array}{c|c}\mathbf{G}^{-1} & \times \\ \hline \times & \times\end{array}\right] \tag{48}$$

where $\mathbf{F}_{11} = \begin{bmatrix}|\xi|^2\|\mathbf{w}_r\|^2 & |\xi|^2\mathrm{Re}\left\{\mathbf{w}_r^{\mathrm{H}}\mathbf{w}_\theta\right\} \\ |\xi|^2\mathrm{Re}\left\{\mathbf{w}_r^{\mathrm{H}}\mathbf{w}_\theta\right\} & |\xi|^2\|\mathbf{w}_\theta\|^2\end{bmatrix}$, $\mathbf{F}_{22} = \|\mathbf{w}\|^2\mathbf{I}_2$, $\mathbf{F}_{12} = \mathbf{F}_{21}^{\mathrm{T}} = \begin{bmatrix}\mathrm{Re}\left\{\mathbf{w}_r^{\mathrm{H}}\mathbf{w}\xi^*\right\} & -\mathrm{Im}\left\{\mathbf{w}_r^{\mathrm{H}}\mathbf{w}\xi^*\right\} \\ \mathrm{Re}\left\{\mathbf{w}_\theta^{\mathrm{H}}\mathbf{w}\xi^*\right\} & -\mathrm{Im}\left\{\mathbf{w}_\theta^{\mathrm{H}}\mathbf{w}\xi^*\right\}\end{bmatrix}$. Thus, we obtain (49) at the bottom of the page. Setting $\mathbf{G} =$

$$\mathbf{F} = K\frac{2E}{N} \times \begin{bmatrix}|\xi|^2\|\mathbf{w}_r\|^2 & |\xi|^2\mathrm{Re}\left\{\mathbf{w}_r^{\mathrm{H}}\mathbf{w}_\theta\right\} & \mathrm{Re}\left\{\mathbf{w}_r^{\mathrm{H}}\mathbf{w}\xi^*\right\} & -\mathrm{Im}\left\{\mathbf{w}_r^{\mathrm{H}}\mathbf{w}\xi^*\right\} \\ |\xi|^2\mathrm{Re}\left\{\mathbf{w}_r^{\mathrm{H}}\mathbf{w}_\theta\right\} & |\xi|^2\|\mathbf{w}_\theta\|^2 & \mathrm{Re}\left\{\mathbf{w}_\theta^{\mathrm{H}}\mathbf{w}\xi^*\right\} & -\mathrm{Im}\left\{\mathbf{w}_\theta^{\mathrm{H}}\mathbf{w}\xi^*\right\} \\ \mathrm{Re}\left\{\mathbf{w}_r^{\mathrm{H}}\mathbf{w}\xi^*\right\} & \mathrm{Re}\left\{\mathbf{w}_\theta^{\mathrm{H}}\mathbf{w}\xi^*\right\} & \|\mathbf{w}\|^2 & 0 \\ -\mathrm{Im}\left\{\mathbf{w}_r^{\mathrm{H}}\mathbf{w}\xi^*\right\} & -\mathrm{Im}\left\{\mathbf{w}_\theta^{\mathrm{H}}\mathbf{w}\xi^*\right\} & 0 & \|\mathbf{w}\|^2\end{bmatrix} \tag{47}$$

$$\mathbf{G} = \mathbf{F}_{11} - \mathbf{F}_{12}\mathbf{F}_{22}^{-1}\mathbf{F}_{21} = |\xi|^2\begin{bmatrix}\|\mathbf{w}_r\|^2 - \frac{\left|\mathbf{w}_r^{\mathrm{H}}\mathbf{w}\right|^2}{\|\mathbf{w}\|^2} & \mathrm{Re}\left\{\mathbf{w}_r^{\mathrm{H}}\mathbf{w}_\theta\right\} - \frac{\mathrm{Re}\left\{\mathbf{w}^{\mathrm{H}}\mathbf{w}_r\mathbf{w}_\theta^{\mathrm{H}}\mathbf{w}\right\}}{\|\mathbf{w}\|^2} \\ \mathrm{Re}\left\{\mathbf{w}_r^{\mathrm{H}}\mathbf{w}_\theta\right\} - \frac{\mathrm{Re}\left\{\mathbf{w}^{\mathrm{H}}\mathbf{w}_r\mathbf{w}_\theta^{\mathrm{H}}\mathbf{w}\right\}}{\|\mathbf{w}\|^2} & \|\mathbf{w}_\theta\|^2 - \frac{\left|\mathbf{w}_\theta^{\mathrm{H}}\mathbf{w}\right|^2}{\|\mathbf{w}\|^2}\end{bmatrix} \tag{49}$$

$|\xi|^2\mathbf{G}_0$, the closed-form CRBs for range and angle as well as coupling relationship are

$$D_r = \frac{N}{2KE|\xi|^2\det(\mathbf{G}_0)}\left(\|\mathbf{w}_\theta\|^2 - \frac{|\mathbf{w}_\theta^{\mathrm{H}}\mathbf{w}|^2}{\|\mathbf{w}\|^2}\right) \tag{50}$$

$$D_\theta = \frac{N}{2KE|\xi|^2\det(\mathbf{G}_0)}\left(\|\mathbf{w}_r\|^2 - \frac{|\mathbf{w}_r^{\mathrm{H}}\mathbf{w}|^2}{\|\mathbf{w}\|^2}\right) \tag{51}$$

$$D_{r\theta} = \frac{N}{2KE|\xi|^2\det(\mathbf{G}_0)}\left(\mathrm{Re}\left\{\mathbf{w}_r^{\mathrm{H}}\mathbf{w}_\theta\right\} - \frac{\mathrm{Re}\left\{\mathbf{w}^{\mathrm{H}}\mathbf{w}_r\mathbf{w}_\theta^{\mathrm{H}}\mathbf{w}\right\}}{\|\mathbf{w}\|^2}\right) \tag{52}$$

where $\det()$ denotes the determinant operator.

Because of the range-angle-dependent characteristic of the transmit steering vector, the FDA-MIMO radar can provide two-dimensional DOFs to realize joint range and angle estimation. In general, if D_r is smaller than $c/(2B)$, the range estimation accuracy is improved in the FDA-MIMO radar. Similarly, the inverse of the FIM can also be expressed as

$$\mathbf{D}_\alpha = \mathbf{F}^{-1} = \frac{N}{2KE}\begin{bmatrix}\mathbf{F}_{11} & \mathbf{F}_{12}\\ \mathbf{F}_{21} & \mathbf{F}_{22}\end{bmatrix}^{-1} = \frac{N}{2KE}\left[\begin{array}{c|c}\times & \times\\ \hline \times & \mathbf{G}'^{-1}\end{array}\right] \tag{53}$$

where $\mathbf{G}' = \mathbf{F}_{22} - \mathbf{F}_{21}\mathbf{F}_{11}^{-1}\mathbf{F}_{12}$. In the sequel, we obtain

$$D_\xi = D_{\breve{\xi}} = \frac{1}{K}\frac{N}{2E|\xi|^4}\frac{1}{\eta} \tag{54}$$

where $\eta = |\mathbf{w}_r^{\mathrm{H}}\mathbf{w}|^2|\mathbf{w}_r|^2 + 2\mathrm{Re}\{\mathbf{w}_r^{\mathrm{H}}\mathbf{w}\mathbf{w}_\theta^{\mathrm{H}}\mathbf{w}\}\mathrm{Re}\{\mathbf{w}_r^{\mathrm{H}}\mathbf{w}_\theta\} + |\mathbf{w}_\theta^{\mathrm{H}}\mathbf{w}|^2|\mathbf{w}_\theta|^2$. The CRBs for range and angle under condition that ξ is known are presented in the Appendix A.

The deterministic CRB can be attained by an efficient estimator if the SNR is sufficiently high and the number of snapshots or pulses is large enough. Under the interference-free environment, i.e., $\mathbf{Q} = \sigma^2\mathbf{I}_{MN}$, the CRB is smaller than that in interference environment. For the interference-free situation, the CRBs for range, angle as well as coupling relationship can be expressed as

$$D_r = \frac{1}{2K\mathrm{SNR}}\frac{12}{MN}\left(\frac{1}{(N^2-1)\kappa_r^2} + \frac{\kappa_{\mathrm{T}}^2}{(M^2-1)\kappa_r^2\kappa_{\mathrm{R}}^2}\right) \tag{55}$$

$$D_\theta = \frac{1}{2K\mathrm{SNR}}\frac{12}{MN(M^2-1)\kappa_{\mathrm{R}}^2} \tag{56}$$

$$D_{r\theta} = -\frac{1}{2K\mathrm{SNR}}\frac{12\kappa_{\mathrm{T}}}{MN(M^2-1)\kappa_r\kappa_{\mathrm{R}}^2} \tag{57}$$

where $\mathrm{SNR} = (E|\xi|^2)/(N\sigma^2)$ is the input SNR, $\kappa_r = 4\pi\Delta f/c$, $\kappa_{\mathrm{R}} = 2\pi d_{\mathrm{R}}\cos(\theta)/\lambda_0$ and $\kappa_{\mathrm{T}} = 2\pi d_{\mathrm{T}}\cos(\theta)/\lambda_0$. The derivation of (55)–(57) is given in Appendix B. It is seen that the CRB for angle is dependent on κ_{R}, i.e., the receive array aperture of the FDA-MIMO radar. Meanwhile, the CRB for range relies on κ_r and the ratio of κ_{R} to κ_{T}. This coincides with the qualitative analysis in Section III. The coupling relationship of range and angle depends on κ_r, κ_{R} and the ratio of κ_{R} to κ_{T}.

Considering the colocated MIMO radar with identical transmit and receive array elements, i.e., $M = N$, $d_{\mathrm{R}} = d_{\mathrm{T}} = d$, $\kappa_r = 4\pi\Delta f/c$, $\kappa_{\mathrm{R}} = \kappa_{\mathrm{T}} = 2\pi d\cos(\theta)/\lambda_0$, we obtain

$$D_r = \frac{1}{2K\mathrm{SNR}}\frac{6}{\pi^2(N^2-1)}\left(\frac{c}{2N\Delta f}\right)^2 \tag{58}$$

$$D_\theta = \frac{1}{2K\mathrm{SNR}}\frac{3\lambda_0^2}{\pi^2\cos^2(\theta)N^2(N^2-1)d^2} \tag{59}$$

Herein, the angle estimation accuracy is mainly related with the array aperture, and that of the range depends on the frequency increment. Obviously, by increasing the frequency increment, more accurate range estimation can be achieved. As analyzed in (42), the upper bound of frequency increment is $B/(2N_a)$. Thus, we have

$$D_r \geq \frac{1}{2K\mathrm{SNR}}\frac{24N_a^2}{\pi^2N^2(N^2-1)}\left(\frac{c}{2B}\right)^2 \tag{60}$$

According to (60), the CRB for range can be decreased by a factor $\sqrt{\frac{1}{2K\mathrm{SNR}}\frac{24N_a^2}{\pi^2N^2(N^2-1)}}$, compared with traditional radar range resolution $c/(2B)$. Thus, the accuracy of the range estimate can be improved.

As aforementioned, the transmit steering vector of the FDA-MIMO radar is both range and angle dependent. The coupling relationship of range and angle parameters is written as

$$D_{r\theta} = -\frac{1}{2K\mathrm{SNR}}\frac{3\lambda_0}{\pi^2\cos(\theta)N^2(N^2-1)d}\left(\frac{c}{2\Delta f}\right) \tag{61}$$

which indicates that the coupling of range and angle parameters is dependent on the angle. Moreover, with the increment of the absolute value of angle, the coupling of range and angle becomes severe. Similarly, the CRB for angle also varies with the angle. However, the CRB for range is unaffected by the range and angle.

TABLE II
PARAMETERS OF FDA-MIMO RADAR

Parameter	Value	Parameter	Value
Reference frequency	10GHz	Element number	10
Frequency increment	301250Hz	Element spacing	0.015m
PRF	5000Hz	Number of pulses	200
Maximun unambiguous range	30km	Ambiguity number	4
Waveform bandwidth	15MHz	Range resolution	10m
Interference angle	30°	INR	30dB

V. SIMULATION RESULTS

In this section, computer simulations are conducted to verify the effectiveness of the proposed unambiguous range and angle estimation method. The simulation parameters are listed in Table II.

Note that the FDA-MIMO radar transmits and receives with the same arrays, i.e., $M = N$. Besides, the frequency increment is optimally chosen according to (42), and q and v are determined using (25). In this simulation, we set $q = 60$ and $v = 0.25$ with $\alpha = 0.1807$.

A. Capon Spectrum Distribution in Joint Transmit-Receive Spatial Frequency Domains

In the first example, we consider the case where two targets are in the range bin under test. The first target is in the first am-

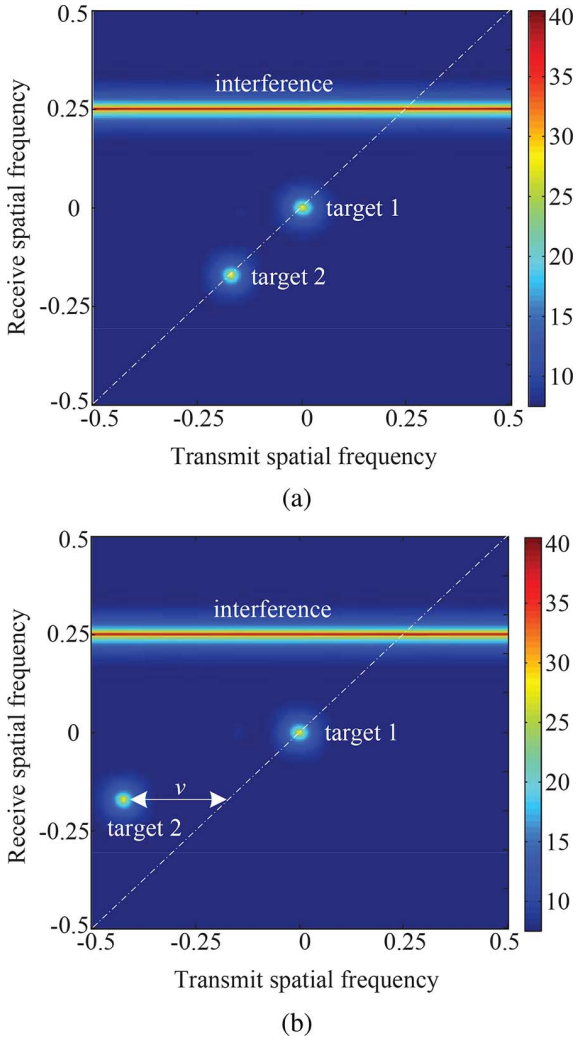

Fig. 4. Spectrum distribution of two targets and interference. (a) Traditional MIMO radar and (b) FDA-MIMO radar.

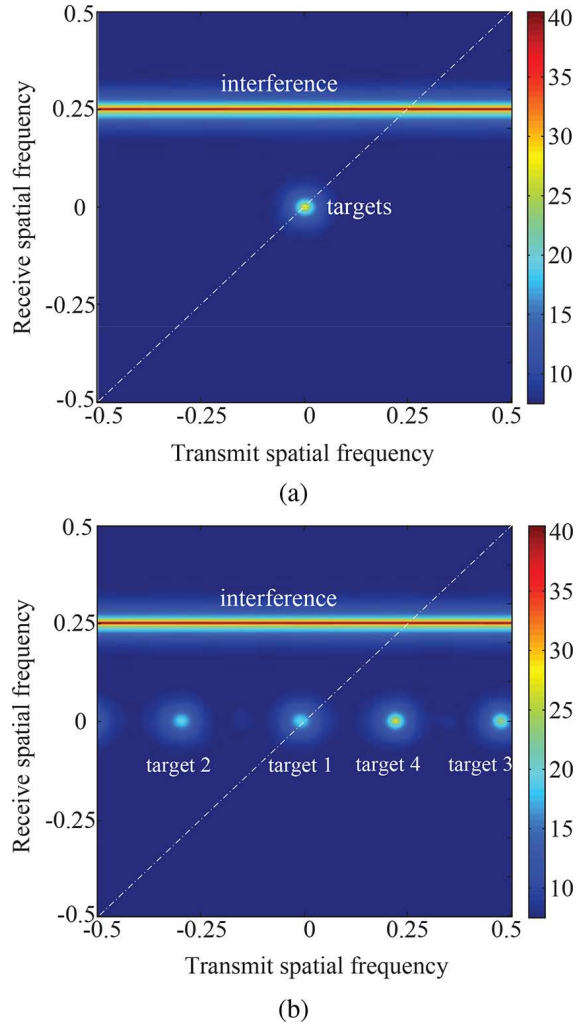

Fig. 5. Spectrum distribution of the four targets and the interference. (a) Traditional MIMO radar and (b) FDA-MIMO radar.

biguous range region (principal range region) while the second target is in the second ambiguous range region. The range bin number is assumed to be 1000. As a result, the *a priori* range estimate r_b is calculated as 10 m $\times 1000 = 10$ km. The angle of the first target is $0°$, while that of the second target is $-20°$. The principal range differences of the targets are both zero. Moreover, the SNRs of the two targets are set as 10 dB.

Figs. 4(a) and (b) show the spectrum distributions of the two targets in interference environment with the traditional MIMO radar and FDA-MIMO radar, respectively. Since the transmit and receive arrays are identical in the traditional MIMO radar, the transmit and receive spatial frequencies of the target are always the same. As shown in Fig. 4(a), the two targets in the traditional MIMO radar are both diagonally distributed. However, in the FDA-MIMO radar, the spectrum distribution of target is no longer diagonally distributed because of the range dependence of the transmit steering vector. As shown in (23), the compensated transmit spatial frequency depends on θ, r_Δ (in this example $r_\Delta = 0$), and p. Since the first target is in the principal range region, its spectrum distribution is also diagonally distributed. In contrast, the second target is in the second ambiguous range region. Hence, the normalized compensated range frequency is $\tilde{f}_{r-\mathrm{comp}} = -(p-1)v = -0.25$. It is seen in Fig. 4(b) that the second target is shifted by a quantity $\tilde{f}_{r-\mathrm{comp}}$ in transmit spatial frequency domain. In addition, the spectrum distribution of the interference is approximately white(independent) in transmit dimension for both the traditional MIMO radar and FDA-MIMO radar.

In the second example, we consider the case in which four targets are in the same range bin and these targets are from the same angle but different ambiguous range regions. The *a priori* range estimate r_b is the same as that in the first example, i.e., $r_b = 10$ km. And the principal range differences of these targets are random variables uniformly distributed on $(-5$ m, 5 m). The SNRs are 0 dB, 0 dB, 5 dB and 10 dB, respectively.

Figs. 5(a) and (b) show the spectrum distributions of the targets in the traditional MIMO radar and FDA-MIMO radar, respectively. Since the four targets share the same angle, they cannot be distinguished in the joint transmit-receive dimensions in the traditional MIMO radar. As can be seen from Fig. 5(a), these four targets overlap in the joint transmit-receive spatial frequency plane. In contrast, the four targets can be distinguished in the FDA-MIMO radar, as shown in Fig. 5(b). As analyzed in Section III.A, the joint transmit-receive spatial frequency plane can be divided into $N_a = 4$ straps. These four targets belong to the 4 straps corresponding to the index of

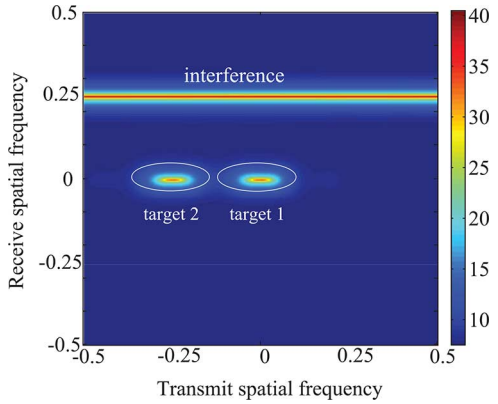

Fig. 6. Spectrum distribution of extended target and interference.

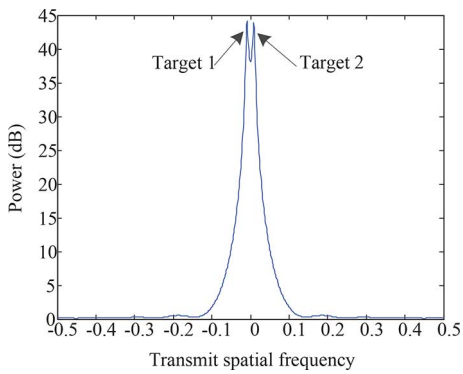

Fig. 7. Resolvability of two point targets in range.

range ambiguity. Note that the number of targets is assumed to *a priori* known or estimated [43], [44].

As aforementioned, the width of each strap results from the principal range difference. Under constraint in (41), these straps are narrow enough to avoid overlapping. In order to verify the effectiveness of (41), Fig. 6 shows the spectrum of two extended targets in FDA-MIMO radar, which are in the first and second ambiguous range regions, respectively. As indicated in Fig. 6, the spectrum of the targets spreads in the transmit dimension. As the width of the spectrum is limited by the second constraint in (41), these two targets can be clearly distinguished. Therefore, the index of range ambiguity can be accurately determined by the proposed approach.

To illustrate the higher range resolution offered by the FDA-MIMO radar, Fig. 7 plots the spectrum of two point targets in the same range bin and the same ambiguous range region. The distance between these two targets equals 5 m. It is seen that the two targets can also be distinguished from each other. Thus, the range resolvability is at least 2 times higher than that in traditional radar for this case.

B. Range and Angle Estimation

In this subsection, we first evaluate the performance of the proposed approach for joint range and angle estimation. To this end, 200 Monte Carlo simulations have been carried out. During the Monte Carlo trials, the sample number is 200, SNR is 0 dB and the angle of the target is 2°. The index of range ambiguity p of the target is randomly chosen from 1 to 4, but fixed for each experiment. The principal range difference r_Δ is also a random variable uniformly distributed between $(-5$ m, 5 m), but fixed for each trial.

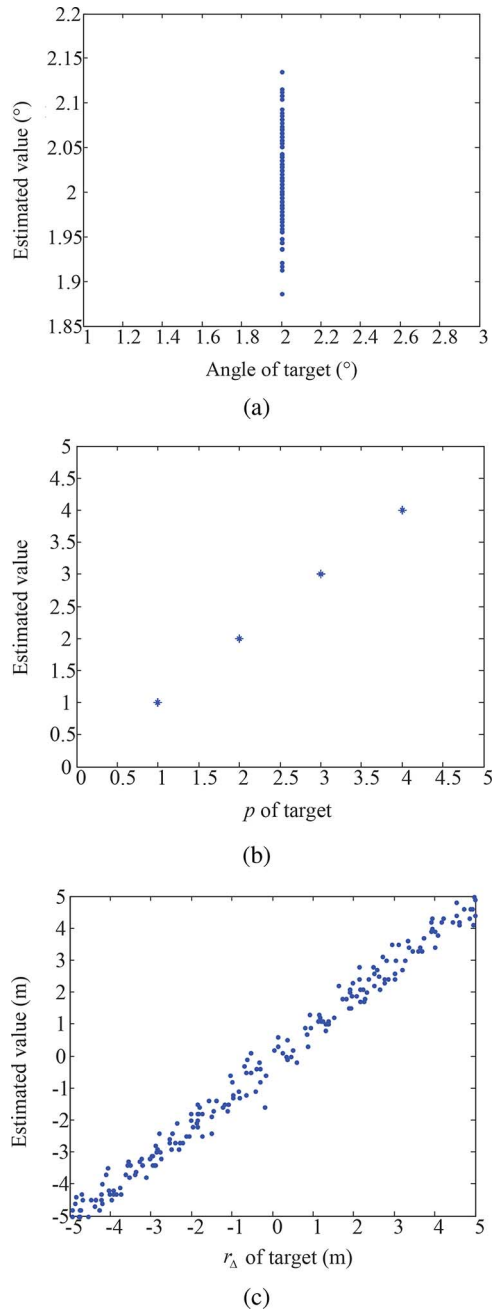

Fig. 8. Parameter estimation results for a target in the presence of interference. (a) Angle estimation, (b) Index of range ambiguity estimation and (c) Principal range difference estimation.

Figs. 8(a), (b) and (c) show the estimation results of the angle, index of range ambiguity and principal range difference, respectively. It is seen from Fig. 8 that the estimated angle is very close to its true value, the estimated indexes of the range ambiguity are exactly equal to their true values, and the estimated principal range differences approach their true counterparts. Therefore, by using the proposed method, the range ambiguity is resolved and the range estimation accuracy can be considerably improved.

The root mean square errors (RMSEs) of the estimates with respect to input SNR are obtained from 200 Monte Carlo trials. Figs. 9 and 10 plot the results under interference and interference-free environments, respectively. Here, the sample number

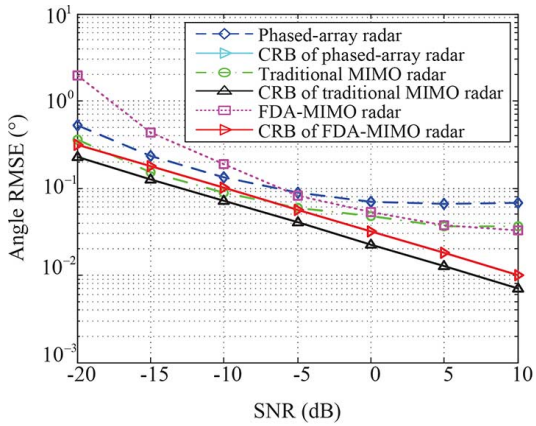

(a)

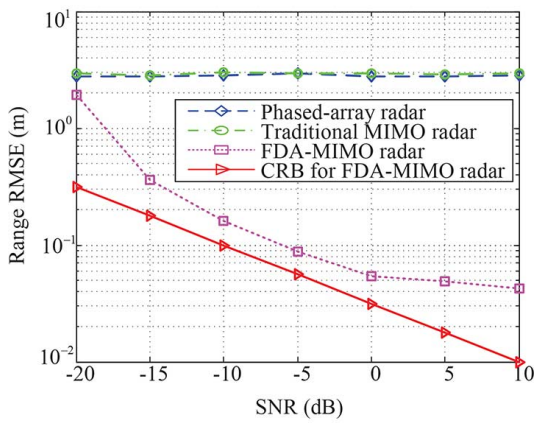

(b)

Fig. 9. RMSE versus SNR in interference environment. (a) Angle estimation and (b) Range estimation.

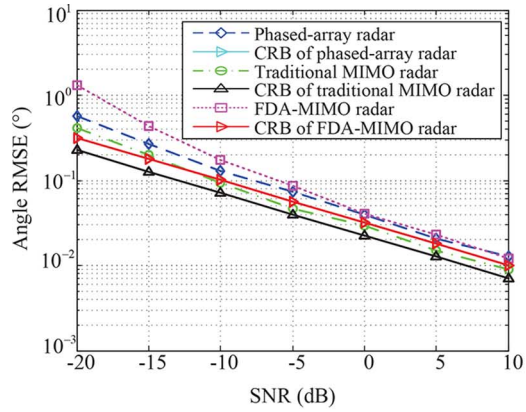

(a)

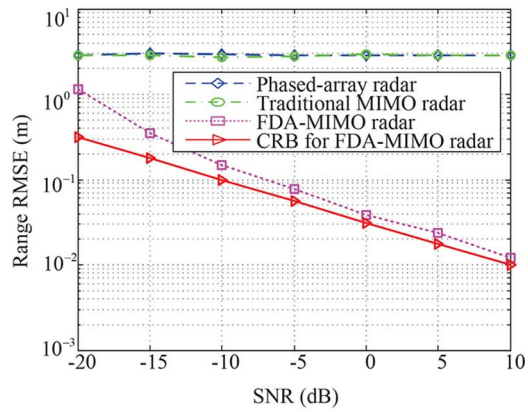

(b)

Fig. 10. RMSE versus SNR in interference-free environment. (a) Angle estimation and (b) Range estimation.

is set as 200. The CRBs are also plotted for comparison. Note that the CRB for angle in the traditional MIMO radar is lower than that for the phased-array radar and FDA-MIMO radar due to the increased aperture of the virtual array in the traditional MIMO radar. It can be observed from Figs. 9(a) and 10(a) that: 1) the angle estimate is biased at high SNRs in the interference environment, 2) the angle estimation accuracy of the FDA-MIMO radar is close to that of the phased-array radar, 3) the RMSEs of the angle estimates are very close to the CRB in the interference-free environment.

Recall that, the transmit spatial frequency of the FDA-MIMO radar is range-dependent, enabling it to further improve the accuracy of the range estimate. It is seen from Figs. 9(b) and 10(b) that the range estimation accuracy can be enhanced with the increase of SNR in the FDA-MIMO radar. However, for the phased-array radar and traditional MIMO radar, the accuracy cannot be improved since the range resolution is determined by the bandwidth of the transmitted waveform, which is fixed in the phased-array radar and traditional MIMO radar. Note that the range ambiguity is not resolved in the phased-array radar and traditional MIMO radar, which therefore is not considered in this experiment. Since the principal range difference of the target is uniformly distributed between $(-5\text{ m}, 5\text{ m})$, the RMSEs of the phased-array radar and traditional MIMO radar are about 2.88 m. In contrast, for the FDA-MIMO radar, the range estimation accuracy is significantly improved. Besides, the range ambiguity in the FDA-MIMO radar can be resolved by the proposed scheme. Similarly, the range estimate is biased at high SNRs under the interference environment.

Figs. 11 and 12 show the RMSEs versus the number of snapshots at SNR $= 0$ dB. It is seen from Fig. 11 that the range and angle estimation accuracies of the FDA-MIMO radar are higher than those of the phased-array radar and traditional MIMO radar in the interference environment. Since the FDA-MIMO radar is able to provide the DOFs in range domain, the range estimation accuracy is improved evidently. As shown in Fig. 12, in the interference-free environment, the RMSEs of angle and range of the FDA-MIMO radar are very close to the CRBs. The performance loss of angle estimation for the FDA-MIMO radar is less than 3 dB compared with the traditional MIMO radar. Moreover, the RMSEs of the range estimates are much smaller in the FDA-MIMO radar than those in the phased-array radar and traditional MIMO radar. Therefore, although the FDA-MIMO radar suffers performance loss in angle estimation, it can provide the super-resolution in range and handle the range ambiguity issue.

C. Root CRB

This subsection is dedicated to the evaluation of the CRBs for a target at angle 0°. In order to show the influence of the interference, the impinging angles of three interferences are set as 30°, 15° and 5° with the interference-to-noise ratio (INR) being equal to 30 dB. The root CRBs for range and angle as well

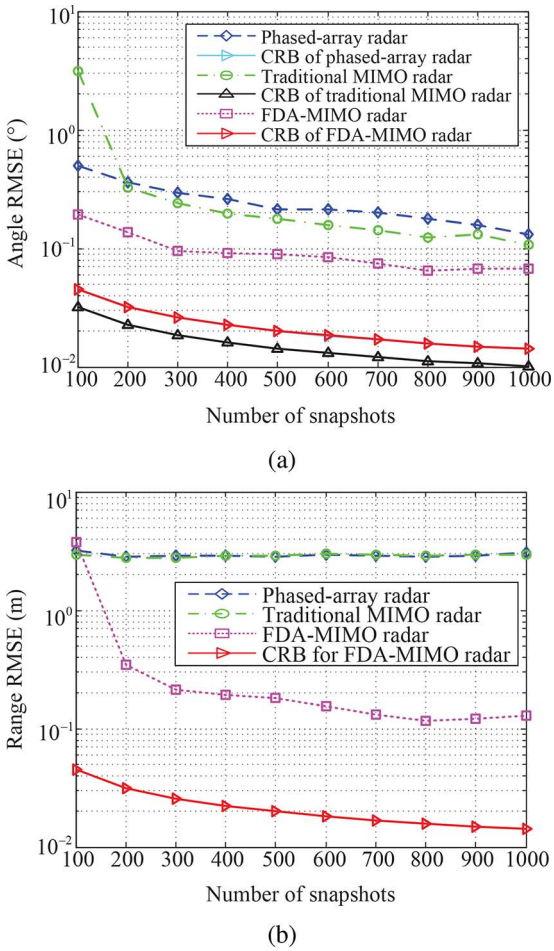

Fig. 11. RMSE versus SNR in interference environment. (a) Angle estimation and (b) Range estimation.

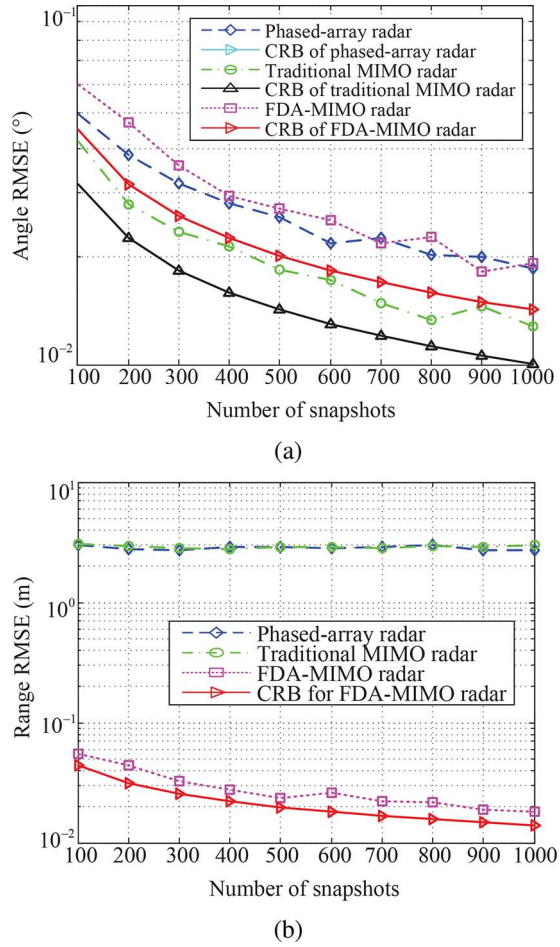

Fig. 12. RMSE versus SNR in interference-free environment. (a) Angle estimation and (b) Range estimation.

as the absolute values of the coupling between range and angle are plotted in Fig. 13. The root CRB in the interference-free environment is lower than that in the interference environment. When the angle of interference is close to that of the target, the root CRBs become larger. It is seen that the root CRB for range is much smaller than the range resolution (10 m) in the interference-free environment.

Equation (42) gives the metric of choosing the optimal frequency increment. To demonstrate the effectiveness of the proposed metric, the root CRB for range is examined versus the value of frequency increment (or the integer q) is depicted in Fig. 14. It is observed that as the frequency increment increases, the range estimation accuracy is improved. However, in order to realize range ambiguity resolution, the frequency increment should be smaller than $B/(2N_a)$. Thus the maximum improvement can be reached when the frequency increment is chosen as the maximum admissible value.

VI. Conclusion

In this paper, an unambiguously joint range and angle estimation approach has been developed utilizing the range-angle-dependent characteristic of the FDA-MIMO radar. In the proposed method, joint range and angle estimation is transformed into a spectrum estimation problem. With the *a priori* knowledge of the target, the range ambiguity can be resolved, and the range estimation accuracy is enhanced evidently. It can be interpreted as determining the angle in the receive spatial domain and then resolving the range ambiguity and estimating the range in the joint transmit-receive spatial frequency domains. Moreover, the optimal scheme for selecting the frequency increment is investigated by introducing the constraint in which the resolvable range ambiguity is guaranteed. Additionally, CRBs for range and angle are derived. For the FDA-MIMO radar, the range estimation accuracy is determined by the frequency increment while the angle estimation accuracy relies on the receive array aperture. The superior performance of the joint range and angle estimation method is validated by extensive simulation results. As a future work, we will explore the diversity of the target RCS and range-angle-dependence of the steering vector. It is expected that not only the target detection performance can be improved, the parameter estimation accuracy will be enhanced.

Appendix A
CRBs for Range and Angle With Knowledge of ξ

If ξ is known, the target parameter vector becomes $\boldsymbol{\alpha} = [r, \theta]^{\mathrm{T}}$. Thus, the CRBs for the range and angle can be expressed as

$$\mathbf{D}_{\boldsymbol{\alpha}}^{-1} = \mathbf{F} = \frac{2KE}{N}|\xi|^2 \mathrm{Re}\left\{\left(\frac{\partial \mathbf{u}(r,\theta)}{\partial \boldsymbol{\alpha}}\right)^{\mathrm{H}} \mathbf{Q}^{-1}\left(\frac{\partial \mathbf{u}(r,\theta)}{\partial \boldsymbol{\alpha}}\right)\right\} \quad (62)$$

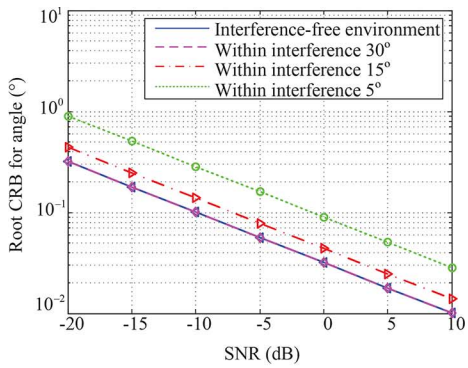

(a)

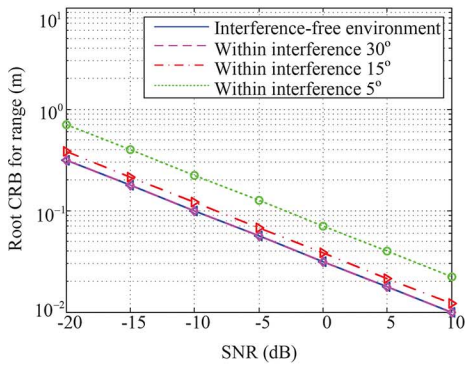

(b)

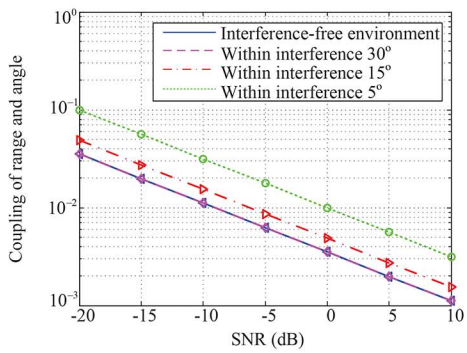

(c)

Fig. 13. Root CRB and coupling versus SNR. (a) Root CRB for angle, (b) Root CRB for range and (c) Coupling of range and angle.

In this case, the FIM can be expressed as

$$\mathbf{F} = \frac{2KE}{N}|\xi|^2 \begin{bmatrix} \|\mathbf{w}_r\|^2 & \mathrm{Re}\left\{\mathbf{w}_r^{\mathrm{H}}\mathbf{w}_\theta\right\} \\ \mathrm{Re}\left\{\mathbf{w}_r^{\mathrm{H}}\mathbf{w}_\theta\right\} & \|\mathbf{w}_\theta\|^2 \end{bmatrix} \tag{63}$$

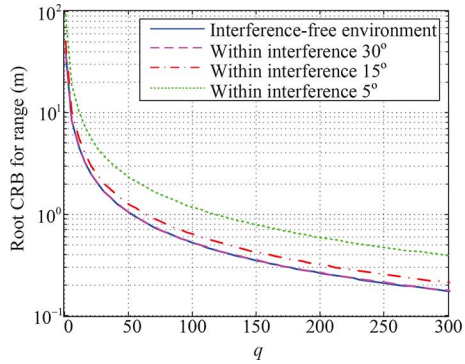

Fig. 14. Root CRB for range versus q.

Thus, the closed-form CRBs for range and angle are

$$D_r = \frac{N}{2KE|\xi|^2} \frac{\|\mathbf{w}_\theta\|^2}{\|\mathbf{w}_r\|^2\|\mathbf{w}_\theta\|^2 - \left(\mathrm{Re}\left\{\mathbf{w}_r^{\mathrm{H}}\mathbf{w}_\theta\right\}\right)^2} \tag{64}$$

$$D_\theta = \frac{N}{2KE|\xi|^2} \frac{\|\mathbf{w}_r\|^2}{\|\mathbf{w}_r\|^2\|\mathbf{w}_\theta\|^2 - \left(\mathrm{Re}\left\{\mathbf{w}_r^{\mathrm{H}}\mathbf{w}_\theta\right\}\right)^2} \tag{65}$$

Appendix B
Determinant of Matrix $\bar{\mathbf{G}}$

In interference-free environment, the CRBs for the parameters of interest can be expressed as

$$\bar{\mathbf{D}}_\alpha = \frac{N}{2E}\left[\frac{1}{\sigma^2}\mathrm{Re}\left\{\left(\frac{\partial \xi \mathbf{u}(r,\theta)}{\partial \alpha}\right)^{\mathrm{H}}\left(\frac{\partial \xi \mathbf{u}(r,\theta)}{\partial \boldsymbol{\alpha}}\right)\right\}\right]^{-1} \tag{66}$$

In this case, we obtain (67) at the bottom of the page. Note that

$$\|\mathbf{u}\|^2 = MN \tag{68}$$

$$\|\mathbf{u}_r\|^2 = \kappa_r^2 M \sum_{n=1}^{N}(n-1)^2 \tag{69}$$

$$\|\mathbf{u}_\theta\|^2 = \kappa_{\mathrm{R}}^2 N \sum_{m=1}^{M}(m-1)^2 + \kappa_{\mathrm{T}}^2 M \sum_{n=1}^{N}(n-1)^2 + 2\kappa_{\mathrm{R}}\kappa_{\mathrm{T}} \sum_{m=1}^{M}(m-1)\sum_{n=1}^{N}(n-1) \tag{70}$$

$$\mathbf{u}_r^{\mathrm{H}}\mathbf{u} = -j\kappa_r M \sum_{n=1}^{N}(n-1) \tag{71}$$

$$\begin{aligned} \bar{\mathbf{G}} &= \frac{|\xi|^2}{\sigma^2}\begin{bmatrix} \|\mathbf{u}_r\|^2 - \frac{|\mathbf{u}_r^{\mathrm{H}}\mathbf{u}|^2}{\|\mathbf{u}\|^2} & \mathrm{Re}\left\{\mathbf{u}_r^{\mathrm{H}}\mathbf{u}_\theta\right\} - \frac{\mathrm{Re}\left\{\mathbf{u}^{\mathrm{H}}\mathbf{u}_r\mathbf{u}_\theta^{\mathrm{H}}\mathbf{u}\right\}}{\|\mathbf{u}\|^2} \\ \mathrm{Re}\left\{\mathbf{u}_r^{\mathrm{H}}\mathbf{u}_\theta\right\} - \frac{\mathrm{Re}\left\{\mathbf{u}^{\mathrm{H}}\mathbf{u}_r\mathbf{u}_\theta^{\mathrm{H}}\mathbf{u}\right\}}{\|\mathbf{u}\|^2} & \|\mathbf{u}_\theta\|^2 - \frac{|\mathbf{u}_\theta^{\mathrm{H}}\mathbf{u}|^2}{\|\mathbf{u}\|^2} \end{bmatrix} \\ &= \frac{|\xi|^2}{\sigma^2}\begin{bmatrix} G_{11} & G_{12} \\ G_{21} & G_{22} \end{bmatrix} \end{aligned} \tag{67}$$

$$\mathbf{u}_\theta^{\mathrm{H}}\mathbf{u} = -j\left[\kappa_{\mathrm{R}}N\sum_{m=1}^{M}(m-1)+\kappa_{\mathrm{T}}M\sum_{n=1}^{N}(n-1)\right] \quad (72)$$

$$\mathbf{u}_r^{\mathrm{H}}\mathbf{u}_\theta = \kappa_{\mathrm{R}}\kappa_r\sum_{m=1}^{M}(m-1)\sum_{n=1}^{N}(n-1) + \kappa_{\mathrm{T}}\kappa_r M\sum_{n=1}^{N}(n-1)^2 \quad (73)$$

where $\kappa_r = 4\pi\Delta f/c$, $\kappa_{\mathrm{R}} = 2\pi d_{\mathrm{R}}\cos(\theta)/\lambda_0$ and $\kappa_{\mathrm{T}} = 2\pi d_{\mathrm{T}}\cos(\theta)/\lambda_0$. Substituting (64)–(69) into (63) yields

$$G_{11} = \frac{MN}{12}(N^2-1)\kappa_r^2 \quad (74)$$

$$G_{22} = \frac{MN}{12}\left[(M^2-1)\kappa_{\mathrm{R}}^2+(N^2-1)\kappa_{\mathrm{T}}^2\right] \quad (75)$$

$$G_{12} = \frac{MN}{12}(N^2-1)\kappa_{\mathrm{T}}\kappa_r \quad (76)$$

And the determinant of the matrix $\bar{\mathbf{G}}$ is computed as

$$\det(\bar{\mathbf{G}}) = \frac{|\xi|^4}{\sigma^4}\kappa_r^2\kappa_{\mathrm{R}}^2\frac{M^2N^2(N^2-1)(M^2-1)}{144} \quad (77)$$

REFERENCES

[1] J. Li and P. Stoica, "MIMO radar with colocated antennas," *IEEE Signal Process. Mag.*, vol. 24, no. 5, pp. 106–114, Sep. 2007.

[2] A. M. Haimovich, R. S. Blum, and L. J. Cimini, "MIMO radar with widely separated antennas," *IEEE Signal Process. Mag.*, vol. 25, no. 1, pp. 116–129, Jan. 2008.

[3] R. Boyer, "Performance bounds and angular resolution limit for the moving colocated MIMO radar," *IEEE Trans. Signal Process.*, vol. 59, no. 4, pp. 1539–1552, Apr. 2011.

[4] M. N. E. Korso, R. Boyer, A. Renaux, and S. Marcos, "Statistical resolution limit for source localization with clutter interference in a MIMO radar context," *IEEE Trans. Signal Process.*, vol. 60, no. 2, pp. 987–992, Feb. 2012.

[5] S. A. Hovanessian, "An algorithm for calculation of range in a multiple PRF radar," *IEEE Trans. Aerosp. Electron. Syst.*, vol. 12, no. 2, pp. 287–290, Mar. 1976.

[6] K. Gerlach and G. A. Andrews, "Cascaded detector for multiple high-PRF pulse Doppler radars," *IEEE Trans. Aerosp. Electron. Syst.*, vol. 26, no. 5, pp. 754–767, Sep. 1990.

[7] G. M. Cleetus, "Properties of staggered PRF radar spectral components," *IEEE Trans. Aerosp. Electron. Syst.*, vol. 12, no. 6, pp. 800–803, Nov. 1976.

[8] D. P. Scholnik, "Range-ambiguous clutter suppression with pulse-diverse waveforms," in *Proc. IEEE Radar Conf.*, Kansas City, MO, USA, May 2011, pp. 336–341.

[9] W.-Q. Wang, C. B. Ding, and X. D. Liang, "Time and phase synchronization via direct-path signal for bistatic synthetic aperture radar systems," *IET Radar Sonar Navig.*, vol. 2, no. 1, pp. 1–11, Feb. 2008.

[10] Y. Yang and R. S. Blum, "Phase synchronization for coherent MIMO radar: Algorithms and their analysis," *IEEE Trans. Signal Process.*, vol. 59, no. 11, pp. 5538–5557, Nov. 2011.

[11] P. Antonik, M. C. Wicks, H. D. Griffiths, and C. J. Baker, "Range-dependent beamforming using element level waveform diversity," in *Proc. Int. Waveform Diversity Design Conf.*, Las Vegas, NV, USA, Jan. 2006, pp. 140–144.

[12] W.-Q. Wang, "Range-angle dependent transmit beampattern synthesis for linear frequency diverse arrays," *IEEE Trans. Antennas Propag.*, vol. 61, no. 8, pp. 4073–4081, Aug. 2013.

[13] M. Secmen, S. Demir, A. Hizal, and T. Eker, "Frequency diverse array antenna with periodic time modulated pattern in range and angle," in *Proc. IEEE Radar Conf.*, Boston, MA, USA, Apr. 2007, pp. 427–430.

[14] T. Eker, S. Demir, and A. Hizal, "Exploitation of linear frequency modulated continuous waveform (LFMCW) for frequency diverse arrays," *IEEE Trans. Antennas Propag.*, vol. 61, no. 7, pp. 3546–3553, Jul. 2013.

[15] J. J. Huang, K. F. Tong, and C. J. Baker, "Frequency diverse array: Simulation and design," in *Proc. IEEE Radar Conf.*, Pasadena, CA, USA, May 2009, pp. 1–4.

[16] J. J. Huang, K. F. Tong, and C. J. Baker, "Frequency diverse array with beam scanning feature," in *Proc. Int. Symp. IEEE Antennas Propag.*, San Diego, CA, USA, Jul. 2008, pp. 1–4.

[17] P. Baizert, T. B. Hale, M. A. Temple, and M. C. Wicks, "Forward-looking radar GMTI benefits using a linear frequency diverse array," *Electron. Lett.*, vol. 42, no. 22, pp. 1311–1312, Oct. 2006.

[18] P. Antonik, M. C. Wicks, H. D. Griffiths, and C. J. Baker, "Multi-mission multi-mode waveform diversity," in *Proc. IEEE Conf. Radar*, Verona, NY, USA, Apr. 2006, pp. 580–582.

[19] P. Antonik, M. C. Wicks, H. D. Griffiths, and C. J. Baker, "Frequency diverse array radars," in *Proc. IEEE Conf. Radar*, Verona, NY, USA, Apr. 2006, pp. 215–217.

[20] T. Higgins, S. D. Blunt, and A. K. Shackelford, "Space-range adaptive processing for waveform-diverse radar imaging," in *Proc. IEEE Radar Conf.*, Washington, DC, USA, May 2010, pp. 321–326.

[21] P. F. Sammartino and C. J. Baker, "Developments in the frequency diverse bistatic system," in *Proc. IEEE Radar Conf.*, Pasadena, CA, USA, May 2009, pp. 1–5.

[22] P. F. Sammartino and C. J. Baker, "The frequency diverse bistatic system," in *Proc. 4th Int. Waveform Diversity Design Conf.*, Kissimmee, FL, USA, Feb. 2009, pp. 155–159.

[23] P. F. Sammartino, C. J. Baker, and H. D. Griffiths, "Range-angle dependent waveform," in *Proc. IEEE Radar Conf.*, Washington, DC, USA, May 2010, pp. 511–515.

[24] P. F. Sammartino, C. J. Baker, and H. D. Griffiths, "Frequency diverse MIMO techniques for radar," *IEEE Trans. Aerosp. Electron. Syst.*, vol. 49, no. 1, pp. 201–222, Jan. 2013.

[25] J. J. Zhang and A. Papandreou-Suppappola, "MIMO radar with frequency diversity," in *Proc. 4th Int. Waveform Diversity Design Conf.*, Kissimmee, FL, USA, Feb. 2009, pp. 208–212.

[26] S. Sen and A. Nehorai, "OFDM MIMO radar with mutual-information waveform design for low-grazing angle tracking," *IEEE Trans. Signal Process.*, vol. 58, no. 6, pp. 3152–3162, Jun. 2010.

[27] W.-Q. Wang and H. Z. Shao, "A flexible phased-MIMO array antenna with transmit beamforming," *Int. J. Antennas Propag.*, pp. 1–10, 2012, Article ID 609598.

[28] W.-Q. Wang, "Phased-MIMO radar with frequency diversity for range-dependent beamforming," *IEEE Sensors J.*, vol. 13, no. 4, pp. 1320–1328, Apr. 2013.

[29] W.-Q. Wang and H. C. So, "Transmit subaperturing for range and angle estimation in frequency diverse array radar," *IEEE Trans. Signal Process.*, vol. 62, no. 8, pp. 2000–2011, Apr. 2014.

[30] W.-Q. Wang and H. Z. Shao, "Range-angle localization of targets by a double-pulse frequency diverse array radar," *IEEE J. Sel. Topics Signal Process.*, vol. 8, no. 1, pp. 1–9, Feb. 2014.

[31] A. Renaux, P. Forster, E. Chaumette, and P. Larzabal, "On the high SNR conditional maximum-likelihood estimator full statistical characterization," *IEEE Trans. Signal Process.*, vol. 54, no. 12, pp. 4840–4843, Dec. 2006.

[32] N. Lehmann, E. Fishler, A. Haimovich, R. Blum, D. Chizhik, L. Cimini, and R. Valenzuela, "Evaluation of transmit diversity in MIMO-radar direction finding," *IEEE Trans. Signal Process.*, vol. 55, no. 5, pp. 2215–2225, May 2007.

[33] I. Bekkerman and J. Tabrikian, "Target detection and localization using MIMO radars and sonars," *IEEE Trans. Signal Process.*, vol. 54, no. 10, pp. 3873–3883, Oct. 2006.

[34] L. Xu, J. Li, and P. Stoica, "Target detection and parameter estimation for MIMO radar systems," *IEEE Trans. Aerosp. Electron. Syst.*, vol. 44, no. 3, pp. 927–939, Jul. 2008.

[35] J. Li, L. Xu, P. Stoica, K. W. Forsythe, and D. W. Bliss, "Range compression and waveform optimization for MIMO radar: A Cramér-Rao bound based study," *IEEE Trans. Signal Process.*, vol. 56, no. 1, pp. 218–232, Jan. 2008.

[36] Q. He, R. S. Blum, and A. M. Haimovich, "Noncoherent MIMO radar for location and velocity estimation: More antennas means better performance," *IEEE Trans. Signal Process.*, vol. 58, no. 7, pp. 3661–3680, Jul. 2010.

[37] J. J. Zhang, G. Maalouli, A. Papandreou-Suppappola, and D. Morrell, "Cramér-Rao lower bounds for the joint estimation of target attributes using MIMO radar," in *Proc. 4th Int. Waveform Diversity Design Conf.*, Kissimmee, FL, USA, Feb. 2009, pp. 103–107.

[38] Y. Wang, W.-Q. Wang, and H. Shao, "Frequency diverse array radar Cramér-Rao lower bounds for estimating direction, range, and velocity," *Int. J. Antennas Propag.*, vol. 2014, pp. 1–15, 2014, Article ID 830869, doi:10.1155/2014/830869.

[39] C. D. Meyer, *Matrix Analysis and Applied Linear Algebra*. Philadelphia, PA, USA: SIAM, 2000.

[40] S. Ahmed, "Product-based pulse integration to combat noise jamming," *IEEE Trans. Aerosp. Electron. Syst.*, vol. 50, no. 3, pp. 2109–2115, Jul. 2014.

[41] Y. C. Eldar, A. Nehorai, and P. S. Rosa, "A competitive mean-squared error approach to beamforming," *IEEE Trans. Signal Process.*, vol. 55, no. 11, pp. 5143–5154, Nov. 2007.
[42] J. Li, P. Stoica, L. Xu, and W. Roberts, "On parameter identifiability of MIMO radar," *IEEE Signal Process. Lett.*, vol. 14, no. 12, pp. 968–971, Dec. 2007.
[43] L. Huang, Q. T. Zhang, and L. L. Cheng, "Information theoretic criterion for stopping turbo iteration," *IEEE Trans. Signal Process.*, vol. 59, no. 2, pp. 848–853, Feb. 2011.
[44] L. Huang, T. Long, and S. J. Wu, "Source enumeration for high-resolution array processing using improved Gerschgorin radii without eigen decomposition," *IEEE Trans. Signal Process.*, vol. 56, no. 12, pp. 5916–5925, Feb. 2008.

Jingwei Xu was born in Shandong. He received the B.S. degree in electrical engineering from Xidian University, Xi'an, China, in 2010. He is currently working toward the Ph.D. degree in the National Key Laboratory of Radar Signal Processing, Xidian University.

His research interests include frequency diverse array, MIMO radar signal processing, robust adaptive beamforming and space-time adaptive processing.

Guisheng Liao (M'96) was born in Guangxi. He received the B.S. degree from Guangxi University, Guangxi, China, and the M.S. and Ph.D. degrees from Xidian University, Xi'an, China, in 1985, 1990, and 1992, respectively.

He is currently a Professor at the National Laboratory of Radar Signal Processing, Xidian University. He has been a Senior Visiting Scholar in the Chinese University of Hong Kong, Hong Kong.

His research interests include array signal processing, space-time adaptive processing, SAR ground moving target indication, and distributed small satellite SAR system design. Dr. Liao is a member of the National Outstanding Person and the Cheung Kong Scholars in China.

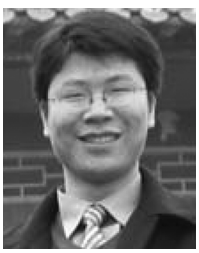

Shengqi Zhu (M'12) was born in Jiangxi. He received the B.S. and Ph.D. degrees in electrical engineering from Xidian University, Xi'an, China, in 2005 and 2010, respectively.

In 2010 he joined Xidian University as a full assistant professor in National Laboratory of Radar Signal Processing where he was promoted to associate professor in 2012. In 2011 and 2014, he was awarded the Young Scientists Award for Excellence in Scientific Research by the International Union of Radio Science (URSI). Currently, he has been the reviewer for IEEE TRANSACTIONS ON AEROSPACE AND ELECTRONIC SYSTEMS, IEEE TRANSACTIONS ON GEOSCIENCE AND REMOTE SENSING, *IET Radar Sonar and Navigation* and so on.

His research interests include space-time adaptive processing, multiple-input multiple-output radar, SAR ground moving target indication and sparse signal processing.

Lei Huang (M'07–SM'14) was born in Guangdong, China. He received the B.Sc., M.Sc., and Ph.D. degrees in electronic engineering from Xidian University, Xian, China, in 2000, 2003, and 2005, respectively.

From 2005 to 2006, he was a Research Associate with the Department of Electrical and Computer Engineering, Duke University, Durham, NC. From 2009 to 2010, he was a Research Fellow with the Department of Electronic Engineering, City University of Hong Kong and a Research Associate with the Department of Electronic Engineering, The Chinese University of Hong Kong. From 2012 to 2014, he was a Full Professor with the Department of Electronic and Information Engineering, Harbin Institute of Technology Shenzhen Graduate School. Since November 2014, he has joined the College of Information Engineering, Shenzhen University, where he is currently a Chair Professor. His research interests include spectral estimation, array signal processing, statistical signal processing, and their applications in radar and wireless communication systems.

He is currently an associate editor of IEEE TRANSACTIONS ON SIGNAL PROCESSING and editorial board member of *Digital Signal Processing*.

Hing Cheung So (S'90–M'95–SM'07–F'15) was born in Hong Kong. He received the B.Eng. degree from the City University of Hong Kong and the Ph.D. degree from The Chinese University of Hong Kong, both in electronic engineering, in 1990 and 1995, respectively.

From 1990 to 1991, he was an Electronic Engineer with the Research and Development Division, Everex Systems Engineering Ltd., Hong Kong. During 1995–1996, he was a Postdoctoral Fellow with The Chinese University of Hong Kong. From 1996 to 1999, he was a Research Assistant Professor with the Department of Electronic Engineering, City University of Hong Kong, where he is currently an Associate Professor. His research interests include statistical signal processing, fast and adaptive algorithms, signal detection, robust estimation, source localization and sparse approximation.

He has been on the editorial boards of *IEEE Signal Processing Magazine* (2014 to present), IEEE TRANSACTIONS ON SIGNAL PROCESSING (2010–2014), *Signal Processing* (2010 to present), and *Digital Signal Processing* (2011 to present). In addition, he is an elected member in Signal Processing Theory and Methods Technical Committee (2011 to present) of the IEEE Signal Processing Society where he is chair in the awards subcommittee (2015 to present). He has been elected Fellow of IEEE in recognition of his contributions to spectral analysis and source localization in 2015.